Diffusive scattering of energetic electrons by intense whistler-mode waves in an inhomogeneous plasma

Journal:	*Journal of Plasma Physics*
Manuscript ID	PLA-2022-0150.R2
Manuscript Type:	Research Article
Date Submitted by the Author:	04-Dec-2022
Complete List of Authors:	Frantsuzov, Viktor; FSBSI Space Research Institute of the Russian Academy of Sciences, Artemyev, Anton; University of California Los Angeles Institute of Geophysics and Planetary Physics, Space plasma physics Zhang, Xiaojia; UCLA Allanson, Oliver; University of Exeter Shustov, Pavel; Institut Kosmiceskih Issledovanij RAN, space plasma physics department Petrukovich, Anatoli; FSBSI Space Research Institute of the Russian Academy of Sciences
Keywords:	Plasma Dynamics, Space Plasma Physics, Plasma Nonlinear Phenomena
Abstract:	Electron resonant interactions with electromagnetic whistler-mode waves play an important role in electron flux dynamics in various space plasma systems: planetary radiation belts, bow shocks, solar wind, and magnetic reconnection regions. Two key wave characteristics determining the regime of wave-particle interactions are the wave intensity and the wave coherency. The classical quasi-linear diffusion approach describes well the electron diffusion by incoherent and low-amplitude waves, whereas the nonlinear resonant models describe electron phase bunching and trapping by highly coherent intense waves. This study is devoted to the investigation of the regime of electron resonant interactions with incoherent but intense waves. Although this regime is characterized by electron diffusion, we show that diffusion rates scale linearly with the wave amplitude, $D \sim B_w$, in contrast to the quasi-linear diffusion scaling $D_{QL} \sim B_w^2$. Using observed wave amplitude distributions, we demonstrate that the quasi-linear diffusion model significantly overestimates electron scattering by incoherent, but intense whistler-mode waves. We discuss obtained results in context of simulations of long-term electron flux dynamics in the space plasma systems.

Under consideration for publication in J. Plasma Phys. 1

Diffusive scattering of energetic electrons by intense whistler-mode waves in an inhomogeneous plasma

Viktor A. Frantsuzov[1,2]†, Anton V. Artemyev[3,1], Xiao-Jia Zhang[3], Oliver Allanson[4], Pavel I. Shustov[1,2], Anatoli A. Petrukovich[1]

[1]Space Research Institute of the Russian Academy of Sciences (IKI), 84/32 Profsoyuznaya Str., Moscow 117997, Russia;

[2]Faculty of Physics, National Research University Higher School of Economics, 21/4 Staraya Basmannaya Ulitsa, Moscow, Russia, 105066;

[3]Institute of Geophysics and Planetary Physics, UCLA, Los Angeles, California 90095, USA;

[4]University of Exeter, Exeter, United Kingdom;

(Received xx; revised xx; accepted xx)

Electron resonant interactions with electromagnetic whistler-mode waves play an important role in electron flux dynamics in various space plasma systems: planetary radiation belts, bow shocks, solar wind, and magnetic reconnection regions. Two key wave characteristics determining the regime of wave-particle interactions are the wave intensity and the wave coherency. The classical quasi-linear diffusion approach describes well the electron diffusion by incoherent and low-amplitude waves, whereas the nonlinear resonant models describe electron phase bunching and trapping by highly coherent intense waves. This study is devoted to the investigation of the regime of electron resonant interactions with incoherent but intense waves. Although this regime is characterized by electron diffusion, we show that diffusion rates scale linearly with the wave amplitude, $D \propto B_w$, in contrast to the quasi-linear diffusion scaling $D_{QL} \propto B_w^2$. Using observed wave amplitude distributions, we demonstrate that the quasi-linear diffusion model significantly overestimates electron scattering by incoherent, but intense whistler-mode waves. We discuss obtained results in context of simulations of long-term electron flux dynamics in the space plasma systems.

1. Introduction

Resonant electron interactions with whistler-mode waves are one of the main drivers of electron pitch-angle scattering and acceleration in various space plasma systems, e.g. solar flares (Bespalov *et al.* 1991; Filatov & Melnikov 2017; Melnikov & Filatov 2020), solar wind (Tong *et al.* 2019; Cattell *et al.* 2020, 2021; Mozer *et al.* 2021), shock waves (Hull *et al.* 2012; Wilson *et al.* 2013; Oka *et al.* 2017; Page *et al.* 2021), planetary radiation belts (Menietti *et al.* 2021; Li *et al.* 2021; Thorne *et al.* 2021), and magnetic reconnection regions (Le Contel *et al.* 2009; Breuillard *et al.* 2016; Zhang *et al.* 2018*a*). The basic theoretical framework for description of such interactions is the quasi-linear model (Vedenov *et al.* 1962; Drummond & Pines 1962; Andronov & Trakhtengerts 1964; Kennel & Engelmann 1966) that is based on the assumption of weak perturbation of particle dynamics by each single resonance. This assumption reduces the Vlasov equation to the Fokker-Plank diffusion equation (Vedenov *et al.* 1962; Drummond & Pines 1962)

† Email address for correspondence: vafrantsuzov@outlook.com

where the main characteristics of wave-particle resonant interactions are diffusion rates. The requirement of a weak perturbation of particle trajectories for a single resonance is equivalent to the requirement that each individual wave-particle resonant interaction should not last for a long time (so particle energy/pitch-angle change for a single resonance is sufficiently small), and there are several mechanisms responsible for particle escape from the resonance.

The original quasi-linear diffusion model assumes the broad spectrum of waves resonating with charged particles (Vedenov *et al.* 1962; Drummond & Pines 1962), when the resonance width in velocity space Δv_R is equal to the difference of resonance v_R velocity (determined for the cyclotron resonant conditions) and wave group velocity $v_g = \partial\omega/\partial k$ (where ω and k are wave frequency and wavenumber). The estimate for the resonance width can be derived from the condition that a change of the resonant particle velocity, $\Delta v_R \sim |v_R - v_g|\Delta k/k$, will remove the particle from the cyclotron resonance (Karpman 1974). The small factor $\Delta k/k$ is determined by the wave spectrum width in wavenumber space, Δk. This mechanism determines the shortness of an individual resonance and justifies the applicability of the diffusion approximation for modeling the dynamics of the charged particle ensemble (Karpman 1974; Le Queau & Roux 1987; Shapiro & Sagdeev 1997). This description works well for low-amplitude whistler-mode waves resonating with electrons in homogeneous systems (without spatial gradients of the background plasma and magnetic field), e.g. in the solar wind (see review by Verscharen *et al.* 2022, and references therein).

The assumption of the background magnetic field homogeneity, however, does not work for many space plasma systems. Resonant electron scattering by whistler-mode waves is often observed in magnetic field traps, regions with a spatially localized minimum of the magnetic field magnitude, where charged particles can be trapped and bouncing. Important examples of such traps are the radiation belt dipole field (Lyons & Williams 1984; Schulz & Lanzerotti 1974) and magnetic holes generated by compressional perturbations on the bow shock (Hull *et al.* 2020; Yao *et al.* 2021; Oka *et al.* 2019). Bouncing within magnetic traps, electrons periodically resonate with whistler-mode waves, and the resonance width for cyclotron resonance in the inhomogeneous field is determined from the condition that a change of the resonant particle velocity (due to the field spatial gradient) $\Delta v_R \sim |\partial v_R/\partial s|/k$ will remove the particle from the cyclotron resonance (Trakhtengerts & Rycroft 2008). If Δv_R is finite, the quasi-linear diffusion model works even for monochromatic waves ($\Delta k \to 0$) resonating with electrons in magnetic traps (Karpman & Shklyar 1977; Shklyar 2021; Albert 2001, 2010). Thus, the only condition required for the application of quasi-linear diffusion model is that the mirror force due to the background magnetic field gradient should be stronger than the Lorentz force of the wave field (Karpman 1974).

The small wave intensity approximation, however, is often violated for whistler-mode waves observed in the highly unstable plasma of shock waves (Zhang *et al.* 1999; Artemyev *et al.* 2022) and plasma injections (Zhang *et al.* 2018*b*, 2019). Such intense waves may resonate with electrons in a nonlinear regime, including effects of phase trapping and phase bunching (e.g., Nunn 1971, 1974; Karpman *et al.* 1974; Inan *et al.* 1978). Although phase bunching is the strongly nonlinear effect (Albert 1993; Bortnik *et al.* 2008), due to the smallness of the electron energy and pitch-angle changes in a single resonant phase bunching, it can be incorporated as a drift term into the Fokker Plank equation (see discussion in Artemyev *et al.* 2014; Allanson *et al.* 2021; Gan *et al.* 2020). Changes of electron energy and pitch-angle due to the phase trapping are comparable to the initial energies/pitch-angles (Omura *et al.* 2007; Summers & Omura 2007), and thus it is not clear how to include this effect into the Fokker-Plank equation. Several approaches with

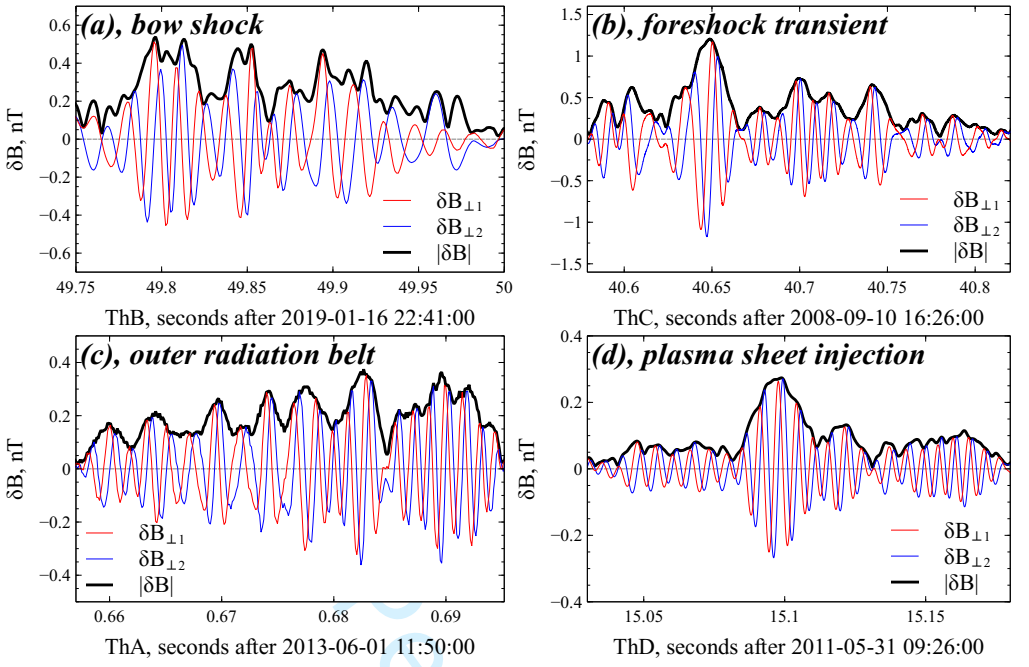

FIGURE 1. Examples of typical wave-packets of whistler-mode waves captured by THEMIS spacecraft Angelopoulos (2008) in the Earth bow shock (a), foreshock transient (b), outer radiation belt (c), plasma injection region (d). These events are picked up from statistics published in (Artemyev *et al.* 2022; Shi *et al.* 2020; Zhang *et al.* 2018*b*,*a*).

different integral operators describing the phase trapping contribution to the electron flux dynamics have been proposed (e.g., Omura *et al.* 2015; Artemyev *et al.* 2018*b*; Vainchtein *et al.* 2018; Hsieh *et al.* 2020), but the evaluation of such operators is computationally expensive and significantly changes the Fokker-Plank equation. Thus, it's important and practically useful to propose an approach for incorporation of nonlinear effects without significant altering models based on the Fokker-Plank equation.

The principal possibility for such an approach has been proposed in Solovev & Shkliar (1986): namely, the total contribution of trapping and bunching may compensate each other. This idea has been reinvestigated in Mourenas *et al.* (2018), where effects of wave modulations were taken into account. Spacecraft observations (e.g., Zhang *et al.* 2019, 2020*b*; Foster *et al.* 2021; Oka *et al.* 2019; Artemyev *et al.* 2022) and numerical simulations (e.g., Nunn & Omura 2012; Katoh & Omura 2016; Demekhov *et al.* 2017; Tao *et al.* 2020; Zhang *et al.* 2021) show that intense whistler-mode waves mostly propagate in a form of short modulated wave-packets. Typical wave-packets include only few wave periods (see Fig. 1), that can be an effect of sideband instability of wave generation (Nunn 1986) or overlapping of several waves with close wave frequencies (Zhang *et al.* 2020*b*; Nunn *et al.* 2021). Such modulation reduces the efficiency of phase trapping (Tao *et al.* 2012*b*, 2013), and can make the net effect of electron resonant interactions with waves more diffusive (Zhang *et al.* 2020*a*; Allanson *et al.* 2020, 2021; Gan *et al.* 2020; An *et al.* 2022; Mourenas *et al.* 2022). Thus, the derivation of diffusion rates is the main question for theoretical description of such regime of wave-particle interaction.

In this paper, we propose an approach for the evaluation of diffusion rates including nonlinear effects for intense, but strongly modulated waves. First, in Section 2 we describe

the concept of the diffusion coefficient model. Then, in Section 3 we provide the basic model equations for the diffusion rate and evaluate diffusion rates for arbitrary wave intensity. Finally, in Section 4 we show the contribution of nonlinear effects on diffusion rates averaged over wave intensity distributions and discuss the obtained results.

2. Basic concept

To propose the approach for the evaluation of such diffusion rate, let us illustrate the wave modulation effect on nonlinear wave-particle interactions. We consider electrons bouncing in a magnetic trap modelled by a curvature-free dipole field (Bell 1984) and their resonant interaction with a monochromatic and intense whistler-mode wave. To evaluate a set of test particle trajectories resonating once with whistler-mode waves, we use the approximation of a monochromatic field-aligned wave. The wave field distribution along the magnetic field lines and the concept of description of wave packets are taken from Mourenas *et al.* (2022). We start with the Hamiltonian of a relativistic electron (rest mass is m_e and charge is $-e$) bouncing in the magnetic trap and interacting with a field-aligned whistler-mode wave:

$$H = \sqrt{\left(\mathbf{p} + \frac{e}{c}\mathbf{A}\right)^2 c^2 + m^2 c^4} \tag{2.1}$$

where $\mathbf{p}$ is a canonical momentum and $\mathbf{A}$ is a vector potential that can be derived from $\mathbf{B} = \nabla \times \mathbf{A}$ with $\mathbf{B} = \mathbf{B}_0 + \mathbf{B}_w$. Here $\mathbf{B}_0$ is the background magnetic field of Earth's dipole and $\mathbf{B}_w$ describes the wave field. As the electron gyroradius is significantly smaller than the dipole magnetic field line curvature, $\sim LR_E$ where R_E is Earth's radius and L-shell, we consider a curvature-free magnetic field with the pair (z, p_z) of Cartesian coordinate and momentum playing a role of field-aligned coordinate and momentum $(s, p_\parallel)$, see Bell (1984). The equatorial magnetic field is determined by a dipole model, $B_0(0) \propto L^{-3}$. To define a $B_0(z)$ function, we introduce a geomagnetic latitude λ:

$$\frac{dz}{d\lambda} = \sqrt{1 + 3\sin^2\lambda}\,\cos\lambda, \quad \frac{B_0(\lambda)}{B_0(0)} = \frac{\sqrt{1 + 3\sin^2\lambda}}{\cos^6\lambda} \tag{2.2}$$

The smallness of electron gyroradius allows us to write $\mathbf{A}_0 = x\widetilde{B}_0(z)\mathbf{e}_y$ ($\mathbf{B}_0 = \nabla \times \mathbf{A}_0$) where $\mathbf{e}_{r_i}$ is the unit vector along the r_i-axis, $r_i = (x, y, z)$, and x is the cross-field coordinate. As the magnetic field $\mathbf{B}_0$ is mainly oriented along the z-axis, we use the approximation $\widetilde{B}_0(z) \approx B_0(z)$. To derive the equation for the wave vector potential $\mathbf{A}_w$, we introduce the wave phase ϕ and define the magnetic vector $\mathbf{B}_w$ as $B_w\mathbf{e}_x\cos\phi - B_w\mathbf{e}_y\sin\phi$. Note B_w may be a function of z (or/and ϕ), but for following derivations we assume that $|dB_w/dz| \ll |(\partial\phi/\partial z)\cdot B_w|$. The wave frequency ω and the wave vector $\mathbf{k}$ are defined by equations $\omega = -\partial\phi/\partial t$ and $\mathbf{k} = \nabla\phi \approx (\partial\phi/\partial z)\mathbf{e}_z$ for field-aligned waves. We consider $\omega = const$ and determine $\mathbf{k}$ from a cold plasma dispersion: $kc/\Omega_{pe} = (\Omega_{ce}/\omega - 1)^{-\frac{1}{2}}$ where $\Omega_{pe} = \sqrt{4\pi n_e e^2/m_e}$ is the plasma frequency and $\Omega_{ce} = eB_0/m_e c$ is the cyclotron frequency (Stix 1962). Therefore, $\mathbf{A}_w \approx B_w\mathbf{e}_x\cos\phi/k - B_w\mathbf{e}_y\sin\phi/k$ and Hamiltonian Eq. 2.1 can be presented as:

$$H = m_e c^2\sqrt{1 + \left(\frac{p_z}{m_e c}\right)^2 + \left(\frac{p_x}{m_e c} + \frac{\Omega_{ce}}{kc}\frac{B_w}{B_0}\cos\phi\right)^2 + \left(\frac{p_y}{m_e c} + \frac{x\Omega_{ce}}{c} - \frac{\Omega_{ce}}{kc}\frac{B_w}{B_0}\sin\phi\right)^2}$$

This Hamiltonian does not depend on y, and thus canonical momentum p_y is a constant: $\dot{p}_y = -\partial H/\partial y = 0$. Without loss of generality, we can set $p_y = 0$.

In the absence of a wave, this Hamiltonian describes fast (x, p_x) oscillations and slow

(z, p_z) oscillations. Thus, we can introduce an adiabatic invariant $I_x = (2\pi)^{-1} \oint dx\, p_x$ as an area surrounded by a closed trajectory in (x, p_x) plane (Landau & Lifshitz 1988):

$$I_x = \frac{1}{2\pi} \oint dx\, p_x = \frac{m_e c^2}{2\Omega_{ce}} \left(\frac{H^2}{m_e^2 c^4} - 1 - \left(\frac{p_z}{m_e c} \right)^2 \right)$$

with

$$H = m_e c^2 \sqrt{1 + \left(\frac{p_z}{m_e c} \right)^2 + \frac{2 I_x \Omega_{ce}}{m_e c^2}}, \quad \frac{2 I_x \Omega_{ce}}{m_e c^2} = \left(\frac{p_x}{m_e c} \right)^2 + \left(\frac{x \Omega_{ce}}{c} \right)^2$$

We consider the canonical transformation $(x, p_x) \to (\psi, I_x)$ given by a generating function $F_2(x,\, I_x) = (2\pi)^{-1} \int dx\, p_x$ (Landau & Lifshitz 1988):

$$F_2(x,\, I_x) = \pm \frac{m_e}{2\pi} \int dx \sqrt{\frac{2 I_x \Omega_{ce}}{m_e} - x^2 \Omega_{ce}^2} = \pm I_x \left[\sqrt{\frac{m_e \Omega_{ce}}{2 I_x}}\, x \sqrt{1 - \frac{m_e \Omega_{ce}}{2 I_x} x^2} + \right.$$
$$\left. + \arcsin \left(\sqrt{\frac{m_e \Omega_{ce}}{2 I_x}}\, x \right) \right]$$

The corresponding variable transformations are

$$p_x = \pm m_e \sqrt{\frac{2 I_x \Omega_{ce}}{m_e} - x^2 \Omega_{ce}^2}, \quad \psi = \pm \arcsin \left(\sqrt{\frac{m_e \Omega_{ce}}{2 I_x}}\, x \right)$$

Thus, equations for x and p_x are

$$x = \frac{c}{\Omega_{ce}} \sqrt{\frac{2 I_x \Omega_{ce}}{m_e c^2}} \sin \psi, \quad p_x = m_e c \sqrt{\frac{2 I_x \Omega_{ce}}{m_e c^2}} \cos \psi$$

A new equation for $\Gamma = H / m_e c^2$ in terms of variables (z, p_z) and (ψ, I_x) can be written as:

$$\Gamma = \sqrt{1 + \left(\frac{p_z}{m_e c} \right)^2 + \frac{2 I_x \Omega_{ce}}{m_e c^2} + 2 \sqrt{\frac{2 I_x \Omega_{ce}}{m_e c^2}} \frac{\Omega_{ce}}{kc} \frac{B_w}{B_0} \cos(\phi + \psi) + \left(\frac{\Omega_{ce}}{kc} \frac{B_w}{B_0} \right)^2} \tag{2.3}$$

The Hamiltonian $H = m_e c^2 \Gamma$ describes the dynamics of two pairs of conjugated variables, (z, p_z) and (ψ, I_x). The system of Hamiltonian equations can be solved with respect to these variables and time t. The general approach consists of expanding H over B_w / B_0, keeping only the linear $\sim B_w / B_0$ term:

$$H = m_e c^2 \gamma + m_e c^2 \sqrt{\frac{2 I_x \Omega_{ce}}{m_e c^2}} \frac{\Omega_{ce}}{\gamma kc} \frac{B_w}{B_0} \cos(\phi + \psi), \quad \gamma = \sqrt{1 + \left(\frac{p_z}{m_e c} \right)^2 + \frac{2 I_x \Omega_{ce}}{m_e c^2}} \tag{2.4}$$

We introduce the wave modulation through the B_w dependence on the wave phase ϕ ($B_w(\phi)$ periodicity mimics effect if multiple wave packets):

$$B_w = B_m \frac{1 - e^{-h \sin^2(\phi / 2l)}}{1 - e^{-h}}, \tag{2.5}$$

where B_m is the peak wave amplitude, l defines the number of wave oscillations (periods) within one wave packet, and h controls the intensity of modulations. The effective wave

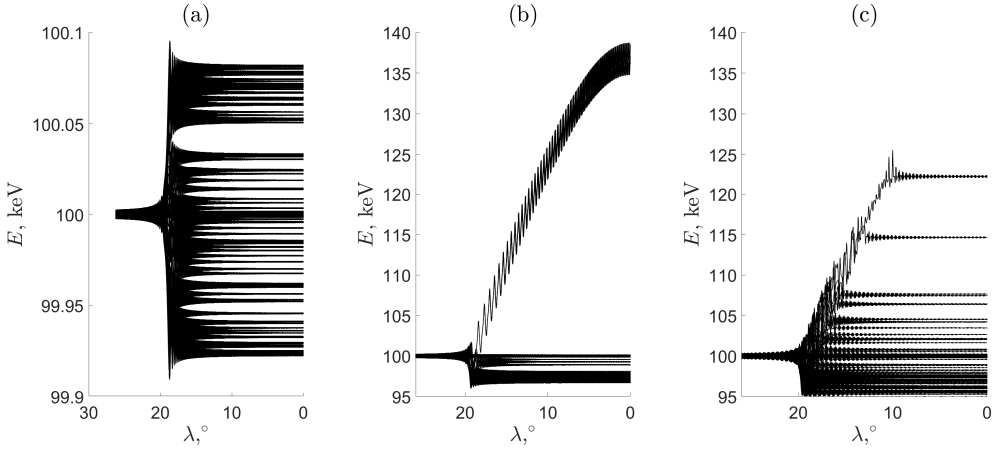

FIGURE 2. A set of trajectories obtained by the numerical integration of Hamiltonian equations for a system (2.4). Results are shown for (a) low amplitude wave with diffusive scattering, for (b) coherent high-amplitude wave with trapping and bunching, (c) modulated high-amplitude wave with diffusive-like scattering. System parameters are: electron energy $E_0 = 100$ keV, equatorial pitch-angle $\alpha_0 = 40°$, number of particles $N = 100$, wave amplitude $B_w = 5$ pT (a), $B_w = 500$ pT (b,c). System parameters correspond to L-shell = 6, whistler-mode waves with the frequency equal to 0.35 of the electron cyclotron frequency at the equator, and the constant plasma frequency equal to 10 of the electron cyclotron frequency at the equator.

amplitude B_{eff} can be determined by averaging B_w over the period of modulations:

$$B_{eff} = \sqrt{\langle B_w^2 \rangle}_{\phi \in [0, 2\pi l]} = B_m \frac{\sqrt{1 - 2I_0\,(h/2)\,e^{-h/2} + I_0\,(h)\,e^{-h}}}{1 - e^{-h}}$$

where $I_n(z)$ is the modified Bessel function of the first kind. The average intensity of the plane wave with $B_w = B_{eff} = const$ equals to the intensity of the modulated wave with B_w given by Eq. (2.5). Thus, to describe the electron diffusion theoretically, the approximation $B_w \approx B_{eff} = const$ can be used. However, this assumption neglects nonlinear effects and, therefore, to determine whether the theory is applicable, we perform numerical simulations modulated waves. Parameter h in Eq. (2.5) determines the *deep* of the modulation: at $h \to \infty$ and $l \to \infty$ wave packet reduces to plane wave. Parameter l determines the wave packet size with the typical values $l \in [10, 30]$ (see Zhang *et al.* 2019, 2021). For numerical simulations we use $h = 1$ and $l = 20$. Note these parameters well satisfy the condition $|dB_w/dz| \ll |(\partial\phi/\partial z) \cdot B_w|$, because $dB_w/dz = (\partial\phi/\partial z) \cdot (dB_w/d\phi)$ and $(dB_w/d\phi)B_w^{-1} \sim h/l \ll 1$.

We consider particles having the same initial energy E_0 and pitch-angle α_0, but random wave phase ϕ and gyrophase ψ. Figure 2 shows typical examples of electron resonance interactions with whistler-mode waves obtained by a numerical integration of Hamiltonian equations: (a) diffusive electron scattering by the low amplitude wave, (b) nonlinear resonant interactions with the intense coherent wave, and (c) nonlinear resonant interactions with the well modulated intense wave. The resonant interaction occurs once per simulation interval (half of the bounce period), i.e. there is only one point along unperturbed particle trajectory where there resonant condition $\dot{\phi} + \dot{\psi} = 0$ is satisfied. The diffusive scattering is characterized by a symmetric (relative to zero) distribution of energy changes, and thus this process should be described by a diffusion rate $\sim \langle (\Delta E)^2 \rangle$. The nonlinear resonances with an intense coherent wave are characterized by a small population changing the energy significantly ($\Delta E > 0$, the phase trapping effect) and

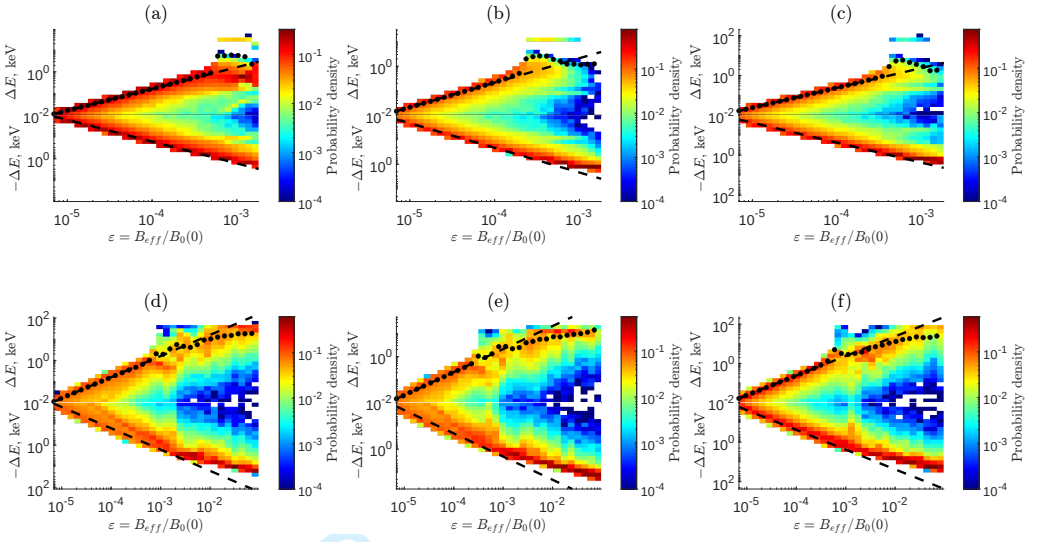

FIGURE 3. Distributions of the energy change ΔE for different B_{eff} with $h = 1$ and $l = 20$ for coherent (top) and modulated (bottom) waves with $\Delta E \propto B_w$ fitting (black dashed lines) and with $\langle(\Delta E)^2\rangle^{1/2}$ profiles (black dots): (a,d) $E_0 = 100$ keV, $\alpha_0 = 40°$, (b,e) $E_0 = 100$ keV, $\alpha_0 = 60°$, (a,f) $E_0 = 300$ keV, $\alpha_0 = 60°$. For each B_w we use 10^4 trajectories to evaluate the ΔE distribution, each particle resonates with the wave only once and ΔE is the energy change for a single resonance, initial particle phases and wave phases are random and thus for a modulated case the actual wave amplitude is different for different particles having the same energy/pitch-angle. For each B_{eff} the ΔE distribution is normalized to one. System parameters correspond to L-shell = 6, whistler-mode waves with the frequency equal to 0.35 of the electron cyclotron frequency at the equator, and the constant plasma frequency equal to 10 of the electron cyclotron frequency at the equator.

a large population with a small, but almost identical for all particles' energy change ($\Delta E < 0$, the phase bunching effect). Thus, nonlinear resonances with a coherent wave should be described separately for trapped and bunched particle populations, and due to the large energy change of the trapped population it is not thought to be possible to include this into the Fokker-Planck equation (see Hsieh & Omura 2017*b*,*a*; Artemyev *et al.* 2021*b*; Zhang *et al.* 2022). The nonlinear resonances with modulated waves are characterized by: (i) an increase of probability for the $\Delta E > 0$ changes; (ii) but also with a decrease in size of $|\Delta E|$ itself; (iii) and further a randomization of energy change for this population. Thus, for modulated waves, the resonant wave-particle interaction is closer to the diffusive scattering (Tao *et al.* 2013; Zhang *et al.* 2020*a*; An *et al.* 2022; Mourenas *et al.* 2022).

In Fig. 3 we show how wave intensity and wave modulation control the efficiency of the nonlinear interactions. The top panels show distributions of energy changes ΔE depending on the normalized wave amplitude $\varepsilon = B_w/B_0(0)$. Below $\varepsilon \sim 10^{-4} - 10^{-3}$ the resonant interaction is diffusive with a symmetrical ΔE distribution and $\langle(\Delta E)^2\rangle^{1/2}$ linearly growing with ε. This dependence $\langle(\Delta E)^2\rangle^{1/2} \propto \varepsilon$ demonstrates the applicability of the unperturbed trajectory approximation, a core assumption of the quasi-linear diffusion theory Tao *et al.* (2011, 2012*a*); Allanson *et al.* (2020). After the wave amplitude reaches a certain threshold (depending on the electron energy, pitch-angle and on system characteristics, see Shklyar & Matsumoto (2009); Omura *et al.* (1991)), the resonant interaction becomes nonlinear with a clear formation of a population of trapped electrons (a separate group of large positive ΔE in the top panels of Fig. 3) and a highly

asymmetrical ΔE distribution (most of the electrons experience the phase bunching and form a large maximum at $\Delta E < 0$). For such nonlinear resonant interactions the ΔE distribution with phase trapped and phase bunched populations cannot be characterized by a diffusion $\langle(\Delta E)^2\rangle$ only, and thus it is not known how to include this regime of resonant interactions into the Fokker-Planck equation.

The bottom panels of Fig. 3 show ΔE distributions as a function of wave amplitude for strongly modulated waves. For small wave intensity, $\varepsilon < 10^{-4}$, there is the same diffusive regime of wave-particle resonant interactions as for non-modulated waves: a symmetrical ΔE distribution with $\langle(\Delta E)^2\rangle^{1/2} \propto \varepsilon$. With the amplitude increase, the regime of wave-particle resonant interaction changes. However, the wave modulation does not allow strong trapping acceleration (there is no population with large positive ΔE), but increases the number of trapped particles (the populations of particles with $\Delta E > 0$ and with $\Delta E < 0$ are comparable even for $\varepsilon > 10^{-3}$). Thus, for intense modulated waves, the ΔE distribution remains almost symmetrical and can be characterized by $\langle(\Delta E)^2\rangle$. Despite such a symmetrical ΔE distribution, the resonant interaction for large ε is nonlinear, and the wave field alters electron dynamics in the resonance. This results in inapplicability of the unperturbed trajectory approximation, and thus $\langle(\Delta E)^2\rangle^{1/2} \propto \varepsilon^A$ with $A < 1$. Therefore, for intense modulated waves we deal with diffusion of resonant electrons, but it is not a quasi-linear diffusion. In this study, we aim to derive the diffusion coefficient $\sim \langle(\Delta E)^2\rangle$ as a function of ε for a wide ε range. The bottom panels of Fig. 3 show that $\langle(\Delta E)^2\rangle$ for small ε should be similar to the quasi-linear diffusion (see also Albert 2010), whereas for large ε the dispersion $\langle(\Delta E)^2\rangle$ should be about $\langle\Delta E\rangle^2$ of phase bunched particle population. We have checked this assumption with an analytical approach, which we further introduce.

3. The diffusion coefficient model for an arbitrary wave intensity

The Hamiltonian $H = m_e c^2 \gamma$ with γ given by Eq. 2.3 determines the electron dynamics. For this Hamiltonian system, we shall derive an analytical approximation for the energy change $\Delta E = m_e c^2 \Delta\gamma$ due to a single resonant interaction. Such change depends on the initial electron energy and pitch-angle, and on the initial phase $\phi + \psi$. Thus, we finally aim to find a mean value $V_\gamma = \langle\Delta\gamma\rangle$ and variance $D_{\gamma\gamma} = \langle(\Delta\gamma)^2\rangle$ with the averaging over initial phases.

To derive the $\Delta\gamma$ equation for $H = m_e c^2 \gamma$, we follow the approach from Neishtadt & Vasiliev (2006); Artemyev *et al.* (2018*a*) for the perturbation theory application to the resonant system containing a phase and a small wave amplitude, $B_w/B_0 \ll 1$ (more precisely, $\varepsilon = B_w/B_0(0) \ll 1$). For analytical consideration we assume that B_w is a constant or a function of the magnetic latitude with the spatial gradient much weaker than wave phase gradients $\partial\phi/\partial s = k$.

The Hamiltonian from Eq. 2.4 is time-dependent as $\phi = \phi(t)$. To find the invariant equation, we define a generation function of the second kind $F_2(s,\, \psi,\, P_z,\, I)$ for $(s,\, p_z,\, \psi,\, I_x) \to (\tilde{z},\, P_z,\, \zeta,\, I)$:

$$F_2(s,\, \psi,\, P_z,\, I) = (\phi + \psi)I + P_z z \qquad \begin{cases} p_z = \frac{\partial F_2}{\partial z} = P_z + kI \\ I_x = \frac{\partial F_2}{\partial \psi} = I \\ \tilde{z} = \frac{\partial F_2}{\partial P_z} = z \\ \zeta = \frac{\partial F_2}{\partial I} = \phi + \psi \\ \mathcal{H} - H = \frac{\partial F_2}{\partial t} = -\omega I \end{cases}$$

As a result, a modified Hamiltonian $\mathcal{H}$ is:

$$\mathcal{H} = m_e c^2 \gamma - \omega I + m_e c^2 \sqrt{\frac{2I\Omega_{ce}}{m_e c^2}} \frac{\Omega_{ce}}{\gamma k c} \frac{B_w}{B_0} \cos\zeta \tag{3.1}$$
$$\gamma = \sqrt{1 + \left(\frac{P_z + kI}{m_e c}\right)^2 + \frac{2I\Omega_{ce}}{m_e c^2}}$$

Note that $\partial_t \mathcal{H} = 0$. Thus, in the zeroth-order of ε the first invariant of this system can be written as:

$$m_e c^2 \gamma - \omega I = const \tag{3.2}$$

Without a wave perturbation, I is invariant ($I = const$) by its definition, and γ has a constant value, considering Eq. 3.2. Thus, all derivatives of those variables are first-order terms of ε or higher. Resonant wave-particle interactions change the particle energy $E = m_e c^2 \gamma$: $\gamma_0 \to \gamma_0 + \Delta\gamma$ where γ_0 is the initial Lorentz factor (at $t = 0$). The resonance equation can be written as $\dot{\zeta} = \partial\mathcal{H}/\partial I = 0$. This equation characterizes the dynamics of the system near the resonance point and, considering Eq. 3.1, can be written down as (subindex R means that the function is evaluated at the resonance):

$$m_e c^2 \left.\frac{\partial\gamma}{\partial I}\right|_R - \omega = 0, \quad \gamma_R = \frac{k_R c}{\omega} \frac{P_z + k_R I_R}{m_e c} + \frac{\Omega_{ce,R}}{\omega} \tag{3.3}$$

The Hamiltonian $\mathcal{H}$ has to be expanded near the resonance point $\dot{\zeta} = 0$ with values $\gamma_R = \gamma_0 + O(\varepsilon)$, $I_R = I_0 + O(\varepsilon)$:

$$\mathcal{H} \approx \mathcal{H}_R + \frac{m_e c^2}{2} \left.\frac{\partial^2\gamma}{\partial I^2}\right|_R (I - I_R)^2 + m_e c^2 \sqrt{\frac{2I_R\Omega_{ce,R}}{m_e c^2}} \frac{\Omega_{ce,R}}{\gamma_R k_R c} \frac{B_w}{B_{0,R}} \cos\zeta \tag{3.4}$$
$$\mathcal{H}_R = m_e c^2 \gamma_R - \omega I_R$$

where

$$\left.\frac{\partial^2\gamma}{\partial I^2}\right|_R = \frac{k_R^2 c^2 - \omega^2}{m_e^2 c^4 \gamma_R}$$

Thus, the final form of $\mathcal{H}$ is

$$\mathcal{H} = \mathcal{H}_R + \frac{(I - I_R)^2}{2g} + m_e c^2 \sqrt{\frac{2I_R\Omega_{ce,R}}{m_e c^2}} \frac{\Omega_{ce,R}}{\gamma_R k_R} \frac{B_w}{B_{0,R}} \cos\zeta \tag{3.5}$$
$$g^{-1} \equiv m_e c^2 \left.\frac{\partial^2\gamma}{\partial I^2}\right|_R = \frac{k_R^2 c^2 - \omega^2}{m_e c^2 \gamma_R}$$

The second term of $\mathcal{H}$ from Eq. 3.5 is an analog of the kinetic energy of the particle motion near the resonance, with $I - I_R$ being the canonical momentum and g playing the role of mass. Thus, we introduce a generating function of the third kind $F_3(\tilde{z}, \tilde{\zeta}, P_z, I)$ for $(z,\ P_z,\ \zeta,\ I) \to (\tilde{z},\ \tilde{P}_z,\ \tilde{\zeta},\ P_\zeta)$:

$$F_3(\tilde{z},\ \tilde{\zeta},\ P_z,\ I) = -(I - I_R)\tilde{\zeta} - P_z \tilde{z}$$

$$\begin{cases} z = -\frac{\partial F_3}{\partial P_z} = \tilde{z} - \frac{\partial I_R}{\partial P_z}\tilde{\zeta} \\ \zeta = -\frac{\partial F_3}{\partial I} = \tilde{\zeta} \\ \tilde{P}_z = -\frac{\partial F_3}{\partial \tilde{z}} = P_z - \frac{\partial I_R}{\partial \tilde{z}}\tilde{\zeta} \\ P_\zeta = -\frac{\partial F_3}{\partial \tilde{\zeta}} = I - I_R \end{cases}$$

As I is an invariant in the unperturbed system, $\partial_{P_z} I_R \sim \varepsilon$ and $\partial_{\tilde{z}} I_R \sim \varepsilon$. This means

that the first term of the Hamiltonian $\mathcal{H}$ can be expanded with respect to ε:

$$\begin{aligned}\mathcal{H}_R = \mathcal{H}_R\left(z,\, P_z\right) = \mathcal{H}_R\left(\tilde{z} - \frac{\partial I_R}{\partial P_z}\zeta,\, \tilde{P}_z + \frac{\partial I_R}{\partial \tilde{z}}\zeta\right) \approx \\ \approx \mathcal{H}_R\left(\tilde{z},\, \tilde{P}_z\right) - \frac{\partial \mathcal{H}_R}{\partial \tilde{z}}\frac{\partial I_R}{\partial \tilde{P}_z}\zeta + \frac{\partial \mathcal{H}_R}{\partial \tilde{P}_z}\frac{\partial I_R}{\partial \tilde{z}}\zeta = \\ = \mathcal{H}_R\left(\tilde{z},\, \tilde{P}_z\right) + \left\{\mathcal{H}_R,\, I_R\right\}_{\tilde{z},\tilde{P}_z}\zeta\end{aligned}$$

Substituting the expanded form of $\mathcal{H}_R$ into Eq. 3.5, we obtain two separate parts of the Hamiltonian $\mathcal{H} = \mathcal{H}_R + \mathcal{H}_\zeta$, $\mathcal{H}_R = m_e c^2\gamma_R - \omega I_R$ with canonical variables $(\tilde{z},\, \tilde{P}_z,\, \zeta,\, P_\zeta)$:

$$\mathcal{H}_\zeta = \frac{P_\zeta^2}{2g} + \left\{\mathcal{H}_R,\, I_R\right\}_{\tilde{z},\tilde{P}_z}\zeta + m_e c^2\sqrt{\frac{2I_R\Omega_{ce,R}}{m_e c^2}}\frac{\Omega_{ce,R}}{\gamma_R k_R c}\frac{B_w}{B_{0,R}}\cos\zeta \tag{3.6}$$

Hamiltonian $\mathcal{H}_R$ describes $(\tilde{z},\, \tilde{P}_z) \approx (z,\, P_z)$ dynamics in the resonance, and this Hamiltonian does not depend on the fast phase ζ. Hamiltonian $\mathcal{H}_\zeta$ is a ζ-dependent pendulum Hamiltonian, that describes fast phase and conjugated momentum dynamics around the resonance. Coefficients of $\mathcal{H}_\zeta$ Hamiltonian depend on $(\tilde{z},\, \tilde{P}_z)$ and slowly change along the resonant trajectory.

In the Hamiltonian $\mathcal{H}_\zeta$, an effective potential energy, $\mathcal{H}_\zeta - P_\zeta^2/2g$, contains two terms: the first term $\sim \{\mathcal{H}_R, I_R\}_{\tilde{z},\tilde{P}_z}$ describes the impact of the background magnetic field gradient and the second term $\sim B_w$ describes the effect of the wave's field. The important system parameter is the ratio of magnitudes of these two terms:

$$a = m_e c^2\sqrt{\frac{2I_R\Omega_{ce,R}}{m_e c^2}}\frac{\Omega_{ce,R}}{\gamma_R k_R c}\frac{B_w}{B_{0,R}}\left\{\mathcal{H}_R,\, I_R\right\}^{-1}_{\tilde{z},\tilde{P}_z} \tag{3.7}$$

Taking into account $\mathcal{H}_R = m_e c^2\gamma_R - \omega I_R$, we can rewrite the Poisson bracket:

$$\left\{\mathcal{H}_R,\, I_R\right\}_{\tilde{z},\tilde{P}_z} = m_e c^2\left\{\gamma_R,\, I_R\right\}_{\tilde{z},\tilde{P}_z} \approx m_e c^2\left\{\gamma_R,\, I_R\right\}_{z,P_z}$$

where γ_R and I_R are given by Eqs. 3.1, 3.3. Combining these equations, we obtain (subindex R is omitted in equations below):

$$\gamma = \frac{kc}{\omega}\frac{P_z + kI}{m_e c} + \frac{\Omega_{ce}}{\omega}, \quad I = \frac{m_e c^2}{2\Omega_{ce}}\left[\gamma^2 - \left(\frac{\omega}{kc}\right)^2\left(\gamma - \frac{\Omega_{ce}}{\omega}\right)^2 - 1\right]$$

Therefore, the Poisson bracket $\{...\} = \{...\}_{s,P_\parallel}$ can be rewritten as:

$$\begin{aligned}\{\gamma,\, I\} = I\Omega_{ce}\left\{\gamma,\, \frac{1}{\Omega_{ce}}\right\} - \frac{m_e c^2}{2\Omega_{ce}}\left\{\gamma,\, \left(\frac{\omega}{kc}\right)^2\left(\gamma - \frac{\Omega_{ce}}{\omega}\right)^2\right\} = -I\frac{\partial\gamma}{\partial P_z}\partial_z\left[\ln\,\Omega_{ce}\right] - \\ - \frac{m_e c^2}{\Omega_{ce}}\frac{\omega}{kc}\left(\gamma - \frac{\Omega_{ce}}{\omega}\right)\left\{\gamma,\, \frac{\omega}{kc}\left(\gamma - \frac{\Omega_{ce}}{\omega}\right)\right\} = -I\frac{\partial\gamma}{\partial P_z}\partial_z\left[\ln\,\Omega_{ce}\right] - \\ - \frac{m_e c^2}{\Omega_{ce}}\frac{\omega}{kc}\left(\gamma - \frac{\Omega_{ce}}{\omega}\right)\left[\left(\gamma - \frac{\Omega_{ce}}{\omega}\right)\frac{\partial\gamma}{\partial P_z}\partial_z\left[\frac{\omega}{kc}\right] - \frac{\omega}{kc}\frac{\Omega_{ce}}{\omega}\frac{\partial\gamma}{\partial P_z}\partial_z\left[\ln\,\Omega_{ce}\right]\right] = \\ = \frac{m_e c^2}{\omega}\frac{\partial\gamma}{\partial P_z}\left[\left(\left(\frac{\omega}{kc}\right)^2\left(\gamma - \frac{\Omega_{ce}}{\omega}\right) - \frac{\omega I}{m_e c^2}\right)\partial_z\left[\ln\,\Omega_{ce}\right] - \frac{\omega}{\Omega_{ce}}\left(\frac{\omega}{kc}\right)^2 \times\right. \\ \left.\times\left(\gamma - \frac{\Omega_{ce}}{\omega}\right)^2\partial_z\left[\ln\,\frac{\omega}{kc}\right]\right]\end{aligned}$$

To determine $\partial_z\left[\ln\,\frac{\omega}{kc}\right]$ we use the cold plasma approximation, $kc/\omega = (\Omega_{pe}/\omega)\cdot(\Omega_{ce}/\omega -$

$1)^{-\frac{1}{2}}$, with constant plasma frequency Ω_{pe}. Therefore, for partial derivatives in $\{\gamma,\, I\}$ we can write:

$$\frac{\partial\gamma}{\partial P_z} = \frac{1}{m_e c}\frac{kc}{\omega}\left(1 + k\frac{\partial I}{\partial P_z}\right), \quad \frac{\partial I}{\partial P_z} = \frac{m_e c^2}{\Omega_{ce}}\frac{\partial\gamma}{\partial P_z}\left[\gamma - \left(\frac{\omega}{kc}\right)^2\left(\gamma - \frac{\Omega_{ce}}{\omega}\right)\right]$$

$$\frac{\partial\gamma}{\partial P_z} = -\frac{1}{\gamma m_e c}\frac{\Omega_{ce}}{\omega}\frac{kc}{\omega}\left[\left(\frac{kc}{\omega}\right)^2 - 1\right]^{-1}, \quad \frac{\partial}{\partial s}\left[\ln\,\frac{\omega}{kc}\right] = \frac{1}{2}\frac{\partial_z\left[ln\;\Omega_{ce}\right]}{1-\omega/\Omega_{ce}}$$

and

$$\{\gamma,\, I\} = \frac{\partial_z\left[ln\;\Omega_{ce}\right]}{\gamma k}\left[\frac{(\gamma-\Omega_{ce}/\omega)^2}{2\,(1-\omega/\Omega_{ce})} - \Omega_{ce}/\omega\left(\gamma - \frac{\Omega_{ce}}{\omega} - \frac{\omega I}{m_e c^2}\left(\frac{kc}{\omega}\right)^2\right)\right]\times$$
$$\times\left[\left(\frac{kc}{\omega}\right)^2 - 1\right]^{-1}$$

Having $\{\gamma,\, I\}$ we can determine a from Eq. 3.7 at the resonance. As we will show, this is the main parameter controlling the energy change due to the resonant wave-particle interaction.

To write an equation for the resonant energy change, $\Delta\gamma$, we use the invariant from Eq. 3.2:

$$\Delta\gamma = \frac{\omega}{m_e c^2}\Delta I = \frac{2\omega}{m_e c^2}\int_{-\infty}^{t_R} dt\,\dot{I} = -\frac{2\omega}{m_e c^2}\int_{-\infty}^{t_R} dt\,\frac{\partial\mathcal{H}}{\partial\zeta} \approx$$
$$\approx 2\omega\sqrt{\frac{2I_R\Omega_{ce,R}}{m_e c^2}}\frac{\Omega_{ce,R}}{\gamma_R k_R c}\frac{B_w}{B_{0,R}}\int_{-\infty}^{\zeta_R} d\zeta\,\frac{\sin\zeta}{\dot{\zeta}} \tag{3.8}$$

where $\Omega_{ce,R} = eB_{0,R}/m_e c$ and $B_{0,R}$ is defined at the resonant $z = z(t_R)$ for given initial energy and pitch-angle. For $\dot{\zeta}$ we use the Hamiltonian equation $\dot{\zeta} = \partial\mathcal{H}_\zeta/\partial P_\zeta$. The resonance is defined by $\dot{\zeta} = P_\zeta/g = 0$ with the solution ζ_R according to $\zeta_R + a\cos\zeta_R = \xi$ with the resonant energy $\xi = \mathcal{H}_\zeta/\{\mathcal{H}_R,\, I_R\}$. Thus, Eq. 3.8 can be written as:

$$\Delta\gamma = 2\omega\sqrt{\frac{gI_R\Omega_{ce,R}}{m_e c^2}}\frac{\Omega_{ce,R}}{\gamma_R k_R c}\frac{B_w}{B_{0,R}}\{\mathcal{H}_R,\, I_R\}^{-1/2}_{\tilde{z},\tilde{P}_z}\int_{-\infty}^{\zeta_R} d\zeta\,\frac{\sin\zeta}{\sqrt{\xi-\zeta-a\,\cos\zeta}} =$$
$$= \left(\frac{2I_R\Omega_{ce,R}}{m_e c^2}\right)^{\frac{1}{4}}\sqrt{\frac{2\Omega_{ce,R}/k_R c}{k_R^2 c^2/\omega^2 - 1}\frac{B_w}{B_{0,R}}}f(a,\xi)$$
$$f(a,\xi) = \int_{-\infty}^{\zeta_R} d\zeta\,\frac{\sqrt{a}\sin\zeta}{\sqrt{\xi-\zeta-a\,\cos\zeta}}$$

Figure 4(a) shows the $f(a,\xi)$ function. This function is periodic with 2π period for ξ (this can be shown analytically, see Appendix A).

The value of ξ varies with the initial conditions, i.e. with wave phase ϕ, gyrophase ψ and electron position on the trajectory in $(s, P_\parallel)$ plane far from the resonance. Assuming a uniform distribution of these parameters, we numerically integrated an ensemble of trajectories as determined by Eqs. 2.4, and so determine the probability function for ξ.

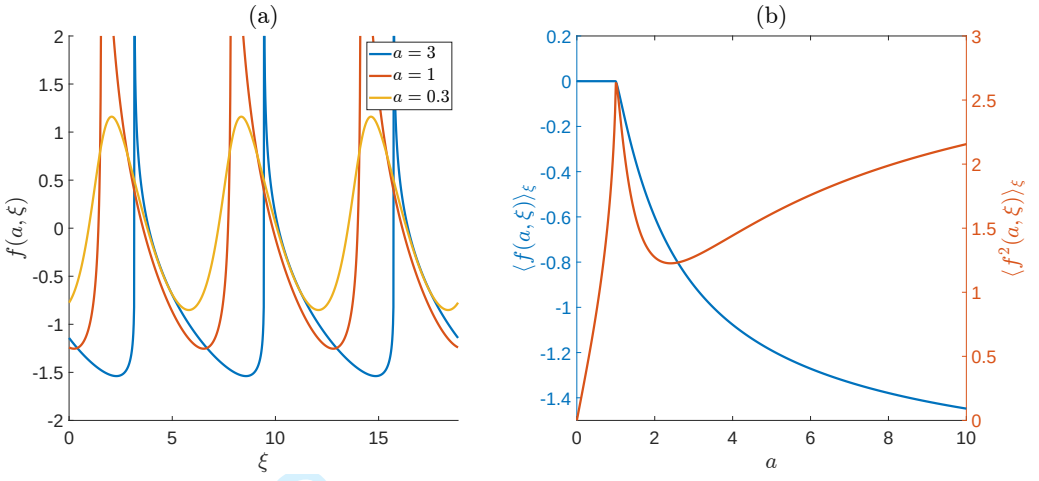

FIGURE 4. Panel (a) show profiles of $f(a,\xi)$ for three a values, and panel (b) shows $\langle f(a,\xi)\rangle_\xi$ and $\langle (f(a,\xi))^2\rangle_\xi$ profiles.

Figure 5 shows such distributions of ξ for three sets of the system parameters. These distributions are very close to the uniform distributions with $\xi \in [0, 2\pi]$, which suggests that averaging over initial parameters ϕ, ψ and s can be substituted with the averaging over ξ with constant weights (see also discussion in Itin *et al.* 2000; Albert *et al.* 2022):

$$\iiint_{\Pi} d\phi\, d\psi\, d\lambda \to \int_{\xi_0}^{\xi_0+2\pi} d\xi, \quad \begin{cases} \xi_0 - \zeta_0 - a\cos\zeta_0 = 0 \\ 1 = a\sin\zeta_0 \end{cases}$$

where Π is the parametric range ($3D$ uniform distribution) and $\xi_0 = \xi_0(a)$ determines the case when the integral diverges near the resonance point (see Appendix A). Thus, the equation for the variance $D_{\gamma\gamma}$ can be written as:

$$D_{\gamma\gamma} = \langle(\Delta\gamma)^2\rangle_\xi = \frac{2\Omega_{ce,R}/k_R c}{k_R^2 c^2/\omega^2 - 1}\frac{B_w}{B_{0,R}}\sqrt{\frac{2I_R\Omega_{ce,R}}{m_e c^2}}\langle f^2(a,\xi)\rangle_\xi$$

where $D_{\gamma\gamma}$ can be considered as a diffusion rate for a unit time interval between two resonant interactions (the actual diffusion rate is the ratio of $\langle D_{\gamma\gamma}\rangle$ and a fraction of electron bounce period).

The function $f(a,\xi)$ determines the difference of the diffusion coefficient $\sim D_{\gamma\gamma}$ and the quasi-linear model. The case of $a \ll 1$, $D_{\gamma\gamma}$ asymptotically tends to the quasi-linear equation $D_{\gamma\gamma} = \langle(\Delta\gamma)^2\rangle \sim (B_w/B_0)^2$ (Albert 2010). To verify that, we have to expand $f(a,\xi)$ in Taylor series:

$$\lim_{a\to 0}\frac{f(a,\xi)}{\sqrt{a}} = \int_{-\infty}^{\xi} d\zeta\,\frac{\sin\zeta}{\sqrt{\xi-\zeta}} = \sqrt{\pi}\,\sin(\xi - \pi/4)$$

$$\lim_{a\to 0}\langle f(a,\xi)\rangle_\xi = 0, \quad \lim_{a\to 0}\frac{\langle f^2(a,\xi)\rangle_\xi}{a} = \frac{\pi}{2}$$

and thus $D_{\gamma\gamma} \propto (B_w/B_0)\langle f^2(a,\xi)\rangle_\xi \propto (B_w/B_0)^2$, because $a \propto B_w/B_0$, see Eq. 3.7.

Figure 4(b) shows that there are two a-ranges with the different wave-particle resonant effects: for $a < 1$ the mean value of $\langle f(a,\xi)\rangle_\xi$ equals zero and there is only a particle diffusion $\propto a\langle f^2(a,\xi)\rangle_\xi$, whereas for $a > 1$ there is a nonzero negative $\langle f(a,\xi)\rangle_\xi$. The

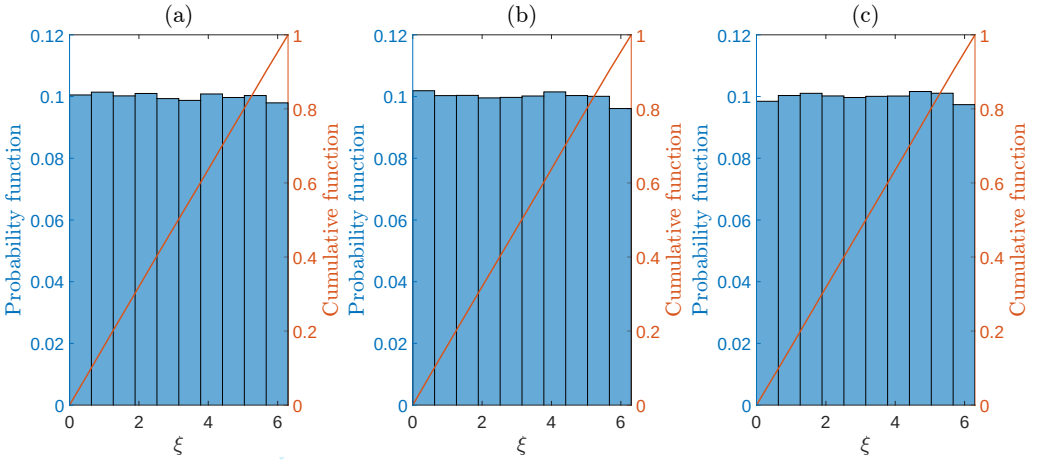

FIGURE 5. Probability distributions of ξ for 10^5 trajectories and (a) $E_0 = 100$ keV, $\alpha_0 = 40°$, $B_w = 50$ pT, (b) $E_0 = 100$ keV, $\alpha_0 = 40°$, $B_w = 500$ pT, (c) $E_0 = 300$ keV, $\alpha_0 = 60°$, $B_w = 500$ pT.

diffusion $\propto a\langle f^2(a,\xi)\rangle_\xi$ has a local maximum at $a \approx 1.0392$, a local minimum at $a \approx 1.5923$, and then increases with a as $\propto a$. The mean value $\langle f(a,\xi)\rangle_\xi$ has an asymptotic $4\sqrt{2}/\pi$ for $a \gg 1$. There is an important property of $f(a,\xi)$: $\langle f^2(a,\xi)\rangle_\xi - \langle f(a,\xi)\rangle_\xi^2 \to 0$ for $a \to \infty$ (see Appendix A for details). This property defines the behavior of the diffusion rate $\propto a\langle f^2(a,\xi)\rangle_\xi$ for $a \gg 1$.

As shown in Fig. 3, the strong wave modulation should result in a symmetric distribution of $\Delta\gamma$ with a zero mean value and with the dispersion $\langle(\Delta\gamma)^2\rangle$ about $\langle(\Delta\gamma)^2\rangle_\xi$ where ξ averaging is performed for population of phase bunched particles (i.e., particles with $\Delta\gamma < 0$). Therefore, for such strongly modulated waves, we shall consider $\langle(\Delta\gamma)^2\rangle_\xi$ as a diffusion rate for both $a < 1$ and $a > 1$ parametric ranges. Figure 6 shows $\langle(\Delta\gamma)^2\rangle_\xi$ distributions in energy, pitch-angle space for three typical wave intensities. Lower energies/higher pitch-angle electrons resonate with waves closer to the equatorial plane, where a is large because $\{\gamma_R,\, I_R\}_{s,P_\parallel} \propto \partial\Omega_{ce}/\partial s$ and tends to zero around the equator.

4. Discussion and conclusions

In this study, we derive the diffusion rate for electrons resonantly interacting with intense whistler-mode waves. Although such intense waves may resonate with electrons nonlinearly, an efficiency of this interaction would be significantly reduced by the wave modulation (Zhang *et al.* 2020*a*; Tao *et al.* 2012*b*; Allanson *et al.* 2021; An *et al.* 2022; Gan *et al.* 2020, 2022). Indeed, most of the intense whistler-mode waves that are observed in space plasma systems (like Earth's radiation belts, bow shock, foreshock transients, and plasma injections) are presented in the form of short well-modulated wave packets (see examples in Fig. 1 and references in the figure caption).

Using test particle simulations, we show that such modulation will reduce the difference between energy changes of phase trapping and phase bunching electrons, and make the energy change distribution more symmetric (see Fig. 3). In the limit of total symmetrization of energy change distribution (extremely modulated wave packets), the main (and the only one) characteristic of electron resonant scattering will be the diffusion rate describing the dispersion of this distribution. Such a diffusion rate can be evaluated

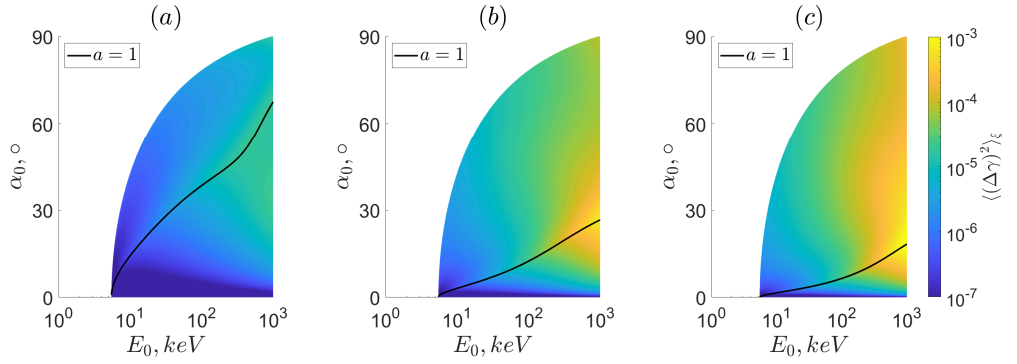

FIGURE 6. 2D energy/pitch-angle maps of (E_0, α_0) for (a) $B_w = 100$ pT, (b) $B_w = 500$ pT, and (c) $B_w = 1000$ pT. Black curve shows $a = 1$.

analytically: the dispersion of the energy changes $\langle(\Delta\gamma)^2\rangle_\xi$ tends to $\langle\Delta\gamma\rangle_\xi^2$ for large wave amplitudes. That is to say, $\langle(\Delta\gamma)^2\rangle_\xi \to \langle\Delta\gamma\rangle_\xi^2 \propto B_w$ for $a \gg 1$ (i.e., when wave amplitude is sufficiently large).

Using this theoretical result, we can calculate the ratio of such a nonlinear diffusion rate and the quasi-linear rate, $\langle(\Delta\gamma)^2\rangle_\xi^{QL} \sim B_w^2$. We can extrapolate to the large wave amplitude limit using a renormalization

$$\langle(\Delta\gamma)^2\rangle_\xi^{QL}(B_w) = \langle(\Delta\gamma)^2\rangle_\xi^{QL}(B_{w,min}) \cdot (B_w/B_{w,min})^2$$

where $B_{w,min}$ corresponds to the $a \ll 1$ limit. The ratio $\langle(\Delta\gamma)^2\rangle_\xi / \langle(\Delta\gamma)^2\rangle_\xi^{QL}$ should show how quasi-linear diffusion models overestimate the diffusion rates for intense waves, because such models scale $\langle(\Delta\gamma)^2\rangle_\xi^{QL}$ with wave intensity B_w^2. Both the numerator and the denominator of this ratio should be weighted with the actual distribution of observed wave intensities, $\mathcal{F}(B_w/B_0)$, and we use two distributions of whistler-mode wave packets collected in the inner magnetosphere.

Figure 7(a) shows two examples of $\mathcal{F}(B_w/B_0)$: the main difference between these distributions is in the definition of wave packets used in the two statistics (see details in Zhang *et al.* (2019, 2020*b*)). Using these distributions, we plot the ratio $\left\langle \langle(\Delta\gamma)^2\rangle_\xi / \langle(\Delta\gamma)^2\rangle_\xi^{QL} \right\rangle_\varepsilon$ as a function of energy and pitch-angle in Fig. 7(b,c). The region with $\left\langle \langle(\Delta\gamma)^2\rangle_\xi / \langle(\Delta\gamma)^2\rangle_\xi^{QL} \right\rangle_\varepsilon \approx 1$ corresponds to the dominant contribution of waves with insufficiently large wave amplitude, where $a < 1$ for most part of ε, and the diffusion rate is $\langle(\Delta\gamma)^2\rangle_\xi \propto B_w^2$. The region with $\left\langle \langle(\Delta\gamma)^2\rangle_\xi / \langle(\Delta\gamma)^2\rangle_\xi^{QL} \right\rangle_\varepsilon < 1$ corresponds to the dominant contribution of high-intensity waves, where $a > 1$ for a significant fraction of the $\mathcal{F}(B_w/B_0)$ distribution, and the diffusion rate $\langle(\Delta\gamma)^2\rangle_\xi \propto B_w$. Note that smaller energy/larger pitch-angle electrons resonate with waves closer to the equator, where $a < 1$ for the larger part of $\mathcal{F}(B_w/B_0)$ distribution.

Figure 7(b,c) demonstrates clearly that the quasi-linear diffusion model significantly overestimates the real diffusion of smaller energy/larger pitch-angle electrons. Note a similar effect of diffusion rate reduction relative to the quasi-linear theory predictions have been obtained for broadband waves (see Tao *et al.* 2011, 2012*a*). This overestimation will be stronger for active geomagnetic conditions with higher wave intensity (Meredith *et al.* 2003, 2012; Agapitov *et al.* 2013, 2018), because $\langle(\Delta\gamma)^2\rangle_\xi / \langle(\Delta\gamma)^2\rangle_\xi^{QL} \propto 1/B_w$. Figures 7(b,c) are plotted under the assumption that there is no net contribution of

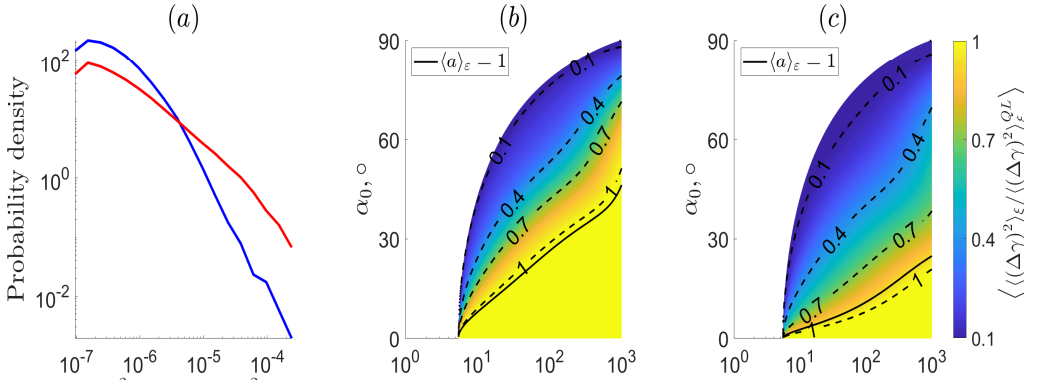

FIGURE 7. (a) Probability distribution functions $\mathcal{F}(B_w/B_0)$ of whistler-mode wave intensities from (Zhang *et al.* 2019) (blue) and (Zhang *et al.* 2020*b*) (red). (b, c) 2D distributions of $\left\langle \langle(\Delta\gamma)^2\rangle_\xi / \langle(\Delta\gamma)^2\rangle_\xi^{QL} \right\rangle_\varepsilon$ in (E_0, α_0) space for two $\mathcal{F}(B_w/B_0)$ distributions from (a).

nonlinear resonant phase bunching and phase trapping effects, and that all wave-particle interactions can be solely described by diffusion because the wave field is dominated by well-modulated short wave packets. The opposite assumption consists of a dominant role of phase trapping and phase bunching effects of electron resonant interactions with coherent long wave packets. For long-term electron dynamics, such effects also can be fitted by diffusion, but the diffusion rate will be much larger than the quasi-linear one (Artemyev *et al.* 2021*a*).

The schematic Figure 8 generalizes both regimes of wave-particle resonant interactions for large-amplitude waves: $\langle(\Delta\gamma)^2\rangle_\xi \propto B_w$ for well-modulated short wave packets and $\langle(\Delta\gamma)^2\rangle_\xi \propto B_w^{1/2}$ for highly coherent long wave packets. For Earth's radiation belts, the quasi-linear simulations of long-term electron flux dynamics generally describe observed electron fluxes with a reasonable tuning of the averaged wave intensity (e.g., Thorne *et al.* 2013; Li *et al.* 2014; Drozdov *et al.* 2015; Ma *et al.* 2018; Allison *et al.* 2021). This will not be possible if any of two limiting cases shown in Fig. 8 would work. Therefore, we shall conclude that wave-particle resonant interactions includes both diffusion by short wave-packets and nonlinear phase trapping/bunching by rare long wave-packets, and a fine balance of these two regimes results in electron diffusion that can be mimicked by the quasi-linear diffusion models. However, for each specific event, such mimicking would require a proper tuning of wave intensity. This underlines the importance of investigations of nonlinear resonant interactions for accurate inclusion of the net effects of phase trapping and phase bunching into wave-particle interaction models.

5. Summary

We have derived the diffusion rate for relativistic electron scattering by intense whistler-mode waves of arbitrary amplitude. This diffusion rate repeats the $D \propto B_w^2$ scaling of the quasi-linear diffusion rate D_{QL} for small amplitudes, and tends to $D \propto B_w$ scaling for amplitudes exceeding the threshold of nonlinear wave-particle interactions. Therefore, under the assumption of the absence of main nonlinear resonant effects (phase trapping and phase bunching) due to low wave coherence, the quasi-linear diffusion model will overestimate the diffusion rate for large amplitude, because $D/D_{QL} \propto B_w^{-1}$. This result demonstrates that the extrapolation of quasi-linear diffusion model should not work for high wave amplitudes, whereas the approximation of the

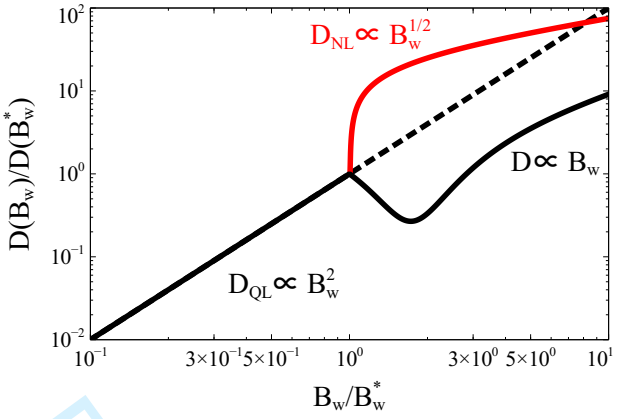

FIGURE 8. A schematic view of diffusion rate scaling with wave amplitude normalized to the amplitude threshold for the nonlinear resonant interactions, B_w^*. Quasi-linear diffusion rate $D_{QL} \propto B_w^2$ works only for $B_w/B_w^* < 1$. For $B_w/B_w^* > 1$ and incoherent waves should work $D \propto B_w$, whereas for coherent waves should work $D_{NL} \propto \sqrt{B_w}$, see Artemyev *et al.* (2021*a*).

total destruction of nonlinear resonant effects (phase trapping and phase bunching) due to low wave coherence/strong wave modulation will underestimate the rates of electron flux dynamics. Thus, for accurate inclusion of statistics of high wave amplitudes into electron flux models, we must account for the contribution of nonlinear resonant effects.

Acknowledgements

Viktor Frantsuzov, Pavel Shustov, and Anatoli Petrukovich acknowledge support from Russian Science Foundation through grant No. 19-12-00313 covering the theoretical part of this work. Anton Artemyev and Xiao-Jia Zhang acknowledge support from NASA HGI 80NSSC22K0522 covering spacecraft data analysis. Oliver Allanson gratefully acknowledges financial support from the University of Exeter, and also from the United Kingdom Research and Innovation (UKRI) Natural Environment Research Council (NERC) Independent Research Fellowship NE/V013963/1.

Appendix A.

This Appendix is devoted to the investigation of the properties of $f(a, \xi)$:

$$f(a,\xi) = \int_{-\infty}^{\zeta_R} d\zeta \, \frac{\sqrt{a}\sin\zeta}{\sqrt{\xi - \zeta - a\,\cos\zeta}}$$

Considering that ξ is a uniformly distributed random variable (see Figure 5), we determine the mean value $\langle f(a,\xi)\rangle_\xi$ and the mean square value $\langle f^2(a,\xi)\rangle_\xi$.

First, let us discuss the convergence of $f(a,\xi)$ integral. At $\zeta \to -\infty$, the function $\sin\zeta/\sqrt{\xi - \zeta - a\,\cos\zeta}$ tends to $\sin\zeta/\sqrt{|\zeta|}$, corresponding to the Fresnel integral, and therefore the integral converges. At $\zeta \to \zeta_R$ the convergence depends on the behavior of

$\xi - \zeta - a\,\cos\zeta$. We introduce $\zeta = \zeta_R - \delta\zeta$ and consider $\delta\zeta$ to be sufficiently small:

$$\begin{aligned}\xi - \zeta - a\,\cos\zeta &= \xi - \zeta_R + \delta\zeta - a\,\cos(\zeta_R - \delta\zeta) \approx \\ &\approx \xi - \zeta_R + \delta\zeta - a\,\cos\zeta_R - a\,\delta\zeta\sin\zeta_R = \\ &= (1 - a\,\sin\zeta_R)\delta\zeta\end{aligned}$$

If $1 - a\,\sin\zeta_R \neq 0$, the integral converges near ζ_R as $\delta\zeta^{-1/2}$. The equation $1 - a\,\sin\zeta_R = 0$ determines cases when $f(a,\xi)$ has an infinite value. Thus, these points have to be excluded from the averaging procedure. By the definition, ζ_R has to be the only solution of $\xi - \zeta - a\,\cos\zeta = 0$ on the interval of integration. Therefore, we expect ζ_R to satisfy the equation $\zeta_R = \arcsin(\frac{1}{a}) + 2\pi n$, where $n \in \mathbb{Z}$. Values of ξ, corresponding to the diverging cases, (noted as ξ_0) can be simply determined from the system of equations:

$$\begin{cases}\xi_0 = \zeta_0 + a\,\cos\zeta_0 \\ 1 = a\,\sin\zeta_0\end{cases}$$

In the case of $a < 1$, there is no solution and the interval of integration for ξ can be performed, i.e. $\xi \in (\pi/2, 5\pi/2)$ (we take $\xi_0(a < 1) \equiv \lim_{a\to 1^+}\xi_0(a) = \pi/2$). For $a \geqslant 1$, this system has infinitely many solutions, separated by 2π. The function $f(a,\xi)$ is periodic with 2π period for ξ:

$$\begin{aligned}f(a,\xi+2\pi) &= \int_{-\infty}^{\zeta_R} d\zeta\,\frac{\sqrt{a}\sin\zeta}{\sqrt{\xi + 2\pi - \zeta - a\,\cos\zeta}} = \int_{-\infty}^{\zeta_R - 2\pi} d\tilde{\zeta}\,\frac{\sqrt{a}\sin\tilde{\zeta}}{\sqrt{\xi - \tilde{\zeta} - a\,\cos\tilde{\zeta}}} = \\ &= \int_{-\infty}^{\tilde{\zeta}_R} d\tilde{\zeta}\,\frac{\sqrt{a}\sin\tilde{\zeta}}{\sqrt{\xi - \tilde{\zeta} - a\,\cos\tilde{\zeta}}} = f(a,\xi)\end{aligned} \tag{A 1}$$

Thus, without a loss of generality, we consider only one value of ξ_0 and the corresponding phase ζ_0. As a result, the mean value $\langle f(a,\xi)\rangle_\xi$ and the mean square value $\langle f^2(a,\xi)\rangle_\xi$ can be defined as:

$$\langle f(a,\xi)\rangle_\xi = \frac{1}{2\pi}\int_{\xi_0}^{\xi_0+2\pi} d\xi \int_{-\infty}^{\zeta_R} d\zeta\,\frac{\sqrt{a}\sin\zeta}{\sqrt{\xi - \zeta - a\,\cos\zeta}} \tag{A 2}$$

$$\langle f^2(a,\xi)\rangle_\xi = \frac{1}{2\pi}\int_{\xi_0}^{\xi_0+2\pi} d\xi \left[\int_{-\infty}^{\zeta_R} d\zeta\,\frac{\sqrt{a}\sin\zeta}{\sqrt{\xi - \zeta - a\,\cos\zeta}}\right]^2 \tag{A 3}$$

To proceed, it is necessary to determine ζ_R as a function of ξ on the interval $(\xi_0, \xi_0 + 2\pi)$:

$$\xi = \zeta_R + a\,\cos\zeta_R \Rightarrow 1 = (1 - a\,\sin\zeta_R)\,\partial_\xi\zeta_R \Rightarrow \partial_\xi\zeta_R = \frac{1}{1 - a\,\cos\zeta_R}$$

$$\lim_{\xi\to\xi_0^+}\zeta_R(a,\xi) = \zeta_m, \qquad \lim_{\xi\to(\xi_0+2\pi)^-}\zeta_R(a,\xi) = \zeta_0 + 2\pi$$

Thus, ζ_R is bounded on the interval $(\zeta_m, \zeta_0 + 2\pi)$ and is monotonic on it, considering the equation for $\partial_\xi\zeta_R$. This implies that the integral interval can be expanded (Neishtadt

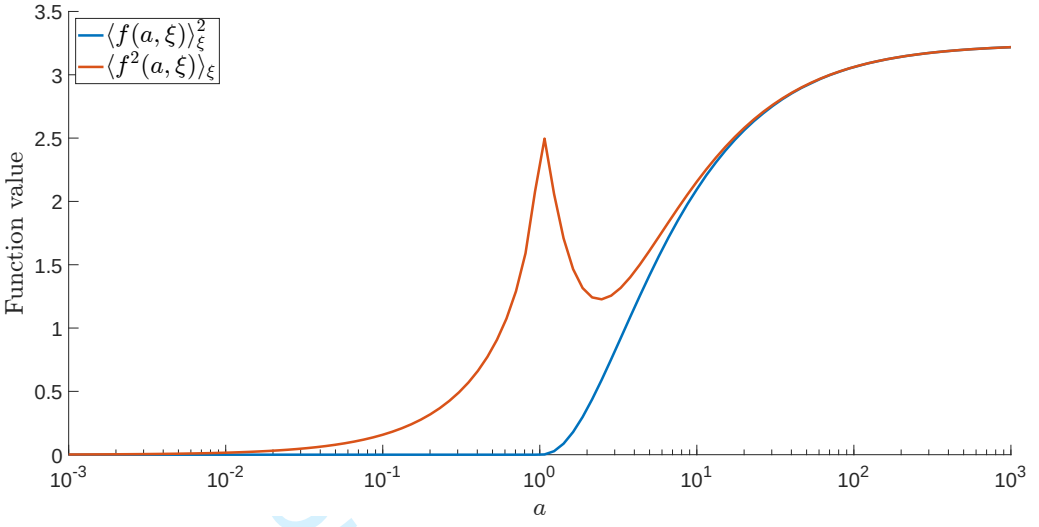

FIGURE 9. Comparison between $\langle f^2(a,\xi)\rangle_\xi$ and $\langle f(a,\xi)\rangle_\xi^2$ as functions of a

1999; Artemyev *et al.* 2018*a*; Albert *et al.* 2022):

$$\langle f(a,\xi)\rangle_\xi = \frac{1}{2\pi}\int\limits_{\xi_0}^{\xi_0+2\pi} d\xi \int\limits_{-\infty}^{\xi_0+2\pi} d\zeta\, \frac{\sqrt{a}\sin\zeta}{\sqrt{\xi-\zeta-a\,\cos\zeta}}\theta(\xi-\zeta-a\,\cos\zeta) =$$

$$= \frac{1}{2\pi}\int\limits_{\xi_0}^{\xi_0+2\pi} d\xi \left[\int\limits_{-\infty}^{\zeta_m} d\zeta\, \frac{\sqrt{a}\sin\zeta}{\sqrt{\xi-\zeta-a\,\cos\zeta}}\theta(\xi-\zeta-a\,\cos\zeta)+\right.$$

$$\left.+\int\limits_{\zeta_m}^{\zeta_0+2\pi} d\zeta\, \frac{\sqrt{a}\sin\zeta}{\sqrt{\xi-\zeta-a\,\cos\zeta}}\theta(\xi-\zeta-a\,\cos\zeta)\right] =$$

$$= \frac{1}{2\pi}\int\limits_{-\infty}^{\zeta_m} d\zeta \int\limits_{\xi_0}^{\xi_0+2\pi} d\xi\, \frac{\sqrt{a}\sin\zeta}{\sqrt{\xi-\zeta-a\,\cos\zeta}} + \frac{1}{2\pi}\int\limits_{\zeta_m}^{\zeta_0+2\pi} d\zeta \int\limits_{\zeta+a\,\cos\zeta}^{\xi_0+2\pi} d\xi\, \frac{\sqrt{a}\sin\zeta}{\sqrt{\xi-\zeta-a\,\cos\zeta}} =$$

$$= \frac{\sqrt{a}}{\pi}\left[-\int\limits_{\zeta_m-2\pi}^{\zeta_m} d\zeta\, \sin\zeta\,\sqrt{\xi_0-\zeta-a\,\cos\zeta} + \int\limits_{\zeta_m}^{\zeta_0+2\pi} d\zeta\, \sin\zeta\,\sqrt{\xi_0+2\pi-\zeta-a\,\cos\zeta}\right] =$$

$$= -\frac{\sqrt{a}}{\pi}\int\limits_{\zeta_0}^{\zeta_m} d\zeta\, \sin\zeta\,\sqrt{\xi_0-\zeta-a\,\cos\zeta} = -\frac{1}{\pi\sqrt{a}}\int\limits_{\zeta_0}^{\zeta_m} d\zeta\sqrt{\xi_0-\zeta-a\,\cos\zeta} =$$

$$= -\frac{1}{\pi\sqrt{a}}\int\limits_{\zeta_0}^{\zeta_m} d\zeta\sqrt{\zeta_0-\zeta+a(\cos\zeta_0-\cos\zeta)} \qquad \text{(A 4)}$$

The integral from Eq. A 4 doesn't have any singularities on the interval of integration and, thus, can be easily computed. To neglect the dependency on ζ_m, an integral in a

complex plane can be introduced:

$$\langle f(a,\xi)\rangle_\xi = -\frac{1}{\pi\sqrt{a}}\,\Re\left[\int_{\zeta_0}^{\zeta_0+2\pi} d\zeta\sqrt{\zeta_0-\zeta+a(\cos\zeta_0-\cos\zeta)}\right]$$

Additionally, Eq. A 4 determines $\langle f(a,\xi)\rangle_\xi$ for $a<1$: $\langle f(a,\xi)\rangle_\xi = 0$ as $\zeta_m = \zeta_0$. For $a\to\infty$ we get:

$$\zeta_0 = \arcsin\left(\frac{1}{a}\right) \Rightarrow \lim_{a\to\infty}\zeta_0 = 0, \quad \lim_{a\to\infty}\zeta_m = 2\pi$$

$$\lim_{a\to\infty}\langle f(a,\xi)\rangle_\xi = -\frac{1}{\pi}\int_0^{2\pi} d\zeta\sqrt{1-\cos\zeta} = -\frac{4\sqrt{2}}{\pi} \tag{A 5}$$

Figure 9 shows that the asymptote $a\gg 1$ is the same for $\langle f^2(a,\xi)\rangle_\xi$ and $\langle f(a,\xi)\rangle_\xi^2$ functions and, considering Eq. (A 5), $\lim_{a\to\infty}\langle f^2(a,\xi)\rangle_\xi = \frac{32}{\pi^2}$.

REFERENCES

Agapitov, O. V., Artemyev, A., Krasnoselskikh, V., Khotyaintsev, Y. V., Mourenas, D., Breuillard, H., Balikhin, M. & Rolland, G. 2013 Statistics of whistler mode waves in the outer radiation belt: Cluster STAFF-SA measurements. *J. Geophys. Res.* **118**, 3407–3420.

Agapitov, O. V., Mourenas, D., Artemyev, A. V., Mozer, F. S., Hospodarsky, G., Bonnell, J. & Krasnoselskikh, V. 2018 Synthetic Empirical Chorus Wave Model From Combined Van Allen Probes and Cluster Statistics. *Journal of Geophysical Research (Space Physics)* **123** (1), 297–314.

Albert, J. M. 1993 Cyclotron resonance in an inhomogeneous magnetic field. *Physics of Fluids B* **5**, 2744–2750.

Albert, J. M. 2001 Comparison of pitch angle diffusion by turbulent and monochromatic whistler waves. *J. Geophys. Res.* **106**, 8477–8482.

Albert, J. M. 2010 Diffusion by one wave and by many waves. *J. Geophys. Res.* **115**, 0.

Albert, J. M., Artemyev, A., Li, W., Gan, L. & Ma, Q. 2022 Analytical results for phase bunching in the pendulum model of wave-particle interactions. *Frontiers in Astronomy and Space Sciences* **9**, 971358.

Allanson, O., Watt, C. E. J., Allison, H. J. & Ratcliffe, H. 2021 Electron Diffusion and Advection During Nonlinear Interactions With Whistler Mode Waves. *Journal of Geophysical Research (Space Physics)* **126** (5), e28793.

Allanson, O., Watt, C. E. J., Ratcliffe, H., Allison, H. J., Meredith, N. P., Bentley, S. N., Ross, J. P. J. & Glauert, S. A. 2020 Particle-in-Cell Experiments Examine Electron Diffusion by Whistler-Mode Waves: 2. Quasi-Linear and Nonlinear Dynamics. *Journal of Geophysical Research (Space Physics)* **125** (7), e27949.

Allison, H. J., Shprits, Y. Y., Zhelavskaya, I. S., Wang, D. & Smirnov, A. G. 2021 Gyroresonant wave-particle interactions with chorus waves during extreme depletions of plasma density in the Van Allen radiation belts. *Science Advances* **7** (5), eabc0380.

An, Z., Wu, Y. & Tao, X. 2022 Electron Dynamics in a Chorus Wave Field Generated From Particle-In-Cell Simulations. *Geophys. Res. Lett.* **49** (3), e97778.

Andronov, A. A. & Trakhtengerts, V. Y. 1964 Kinetic instability of the Earth's outer radiation belt. *Geomagnetism and Aeronomy* **4**, 233–242.

Angelopoulos, V. 2008 The THEMIS Mission. *Space Sci. Rev.* **141**, 5–34.

Artemyev, A. V., Neishtadt, A. I., Vainchtein, D. L., Vasiliev, A. A., Vasko, I. Y. & Zelenyi, L. M. 2018*a* Trapping (capture) into resonance and scattering on resonance: Summary of results for space plasma systems. *Communications in Nonlinear Science and Numerical Simulations* **65**, 111–160.

Artemyev, A. V., Neishtadt, A. I., Vasiliev, A. A. & Mourenas, D. 2018*b* Long-term

evolution of electron distribution function due to nonlinear resonant interaction with whistler mode waves. *Journal of Plasma Physics* **84**, 905840206.

Artemyev, A. V., Neishtadt, A. I., Vasiliev, A. A. & Mourenas, D. 2021*a* Transitional regime of electron resonant interaction with whistler-mode waves in inhomogeneous space plasma. *Phys. Rev. E* **104** (5), 055203, arXiv: 2107.13511.

Artemyev, A. V., Neishtadt, A. I., Vasiliev, A. A., Zhang, X.-J., Mourenas, D. & Vainchtein, D. 2021*b* Long-term dynamics driven by resonant wave-particle interactions: from Hamiltonian resonance theory to phase space mapping. *Journal of Plasma Physics* **87** (2), 835870201, arXiv: 2011.00208.

Artemyev, A. V., Shi, X., Liu, T. Z., Zhang, X. J., Vasko, I. & Angelopoulos, V. 2022 Electron Resonant Interaction With Whistler Waves Around Foreshock Transients and the Bow Shock Behind the Terminator. *Journal of Geophysical Research (Space Physics)* **127** (2), e29820.

Artemyev, A. V., Vasiliev, A. A., Mourenas, D., Agapitov, O. V. & Krasnoselskikh, V. V. 2014 Electron scattering and nonlinear trapping by oblique whistler waves: The critical wave intensity for nonlinear effects. *Physics of Plasmas* **21** (10), 102903.

Bell, T. F. 1984 The nonlinear gyroresonance interaction between energetic electrons and coherent VLF waves propagating at an arbitrary angle with respect to the earth's magnetic field. *J. Geophys. Res.* **89**, 905–918.

Bespalov, P. A., Zaitsev, V. V. & Stepanov, A. V. 1991 Consequences of Strong Pitch-Angle Diffusion of Particles in Solar Flares. *Astrophys. J.* **374**, 369.

Bortnik, J., Thorne, R. M. & Inan, U. S. 2008 Nonlinear interaction of energetic electrons with large amplitude chorus. *Geophys. Res. Lett.* **35**, 21102.

Breuillard, H., Le Contel, O., Retino, A., Chasapis, A., Chust, T., Mirioni, L., Graham, D. B., Wilder, F. D., Cohen, I., Vaivads, A., Khotyaintsev, Y. V., Lindqvist, P.-A., Marklund, G. T., Burch, J. L., Torbert, R. B., Ergun, R. E., Goodrich, K. A., Macri, J., Needell, J., Chutter, M., Rau, D., Dors, I., Russell, C. T., Magnes, W., Strangeway, R. J., Bromund, K. R., Plaschke, F., Fischer, D., Leinweber, H. K., Anderson, B. J., Le, G., Slavin, J. A., Kepko, E. L., Baumjohann, W., Mauk, B., Fuselier, S. A. & Nakamura, R. 2016 Multispacecraft analysis of dipolarization fronts and associated whistler wave emissions using MMS data. *Geophys. Res. Lett.* **43**, 7279–7286.

Cattell, C., Short, B., Breneman, A., Halekas, J., Whittesley, P., Larson, D., Kasper, J. C., Stevens, M., Case, T., Moncuquet, M., Bale, S., Bonnell, J., Dudok de Wit, T., Goetz, K., Harvey, P., MacDowall, R., Malaspina, D., Maksimovic, M., Pulupa, M. & Goodrich, K. 2021 Narrowband oblique whistler-mode waves: comparing properties observed by Parker Solar Probe at < 0.3 AU and STEREO at 1 AU. *Astronomy & Astrophysics* **650**, A8, arXiv: 2009.05629.

Cattell, C. A., Short, B., Breneman, A. W. & Grul, P. 2020 Narrowband Large Amplitude Whistler-mode Waves in the Solar Wind and Their Association with Electrons: STEREO Waveform Capture Observations. *Astrophys. J.* **897** (2), 126, arXiv: 2003.09659.

Demekhov, A. G., Taubenschuss, U. & Santolík, O. 2017 Simulation of VLF chorus emissions in the magnetosphere and comparison with THEMIS spacecraft data. *J. Geophys. Res.* **122**, 166–184.

Drozdov, A. Y., Shprits, Y. Y., Orlova, K. G., Kellerman, A. C., Subbotin, D. A., Baker, D. N., Spence, H. E. & Reeves, G. D. 2015 Energetic, relativistic, and ultrarelativistic electrons: Comparison of long-term VERB code simulations with Van Allen Probes measurements. *J. Geophys. Res.* **120**, 3574–3587.

Drummond, W. E. & Pines, D. 1962 Nonlinear stability of plasma oscillations. *Nuclear Fusion Suppl.* **3**, 1049–1058.

Filatov, L. V. & Melnikov, V. F. 2017 Influence of Whistler Turbulence on Fast Electron Distribution and Their Microwave Emissions in a Flare Loop. *Geomagnetism and Aeronomy* **57** (8), 1001–1008.

Foster, J. C., Erickson, P. J. & Omura, Y. 2021 Subpacket structure in strong VLF chorus rising tones: characteristics and consequences for relativistic electron acceleration. *Earth, Planets and Space* **73** (1), 140.

Gan, L., Li, W., Ma, Q., Albert, J. M., Artemyev, A. V. & Bortnik, J. 2020 Nonlinear

Interactions Between Radiation Belt Electrons and Chorus Waves: Dependence on Wave Amplitude Modulation. *Geophys. Res. Lett.* **47** (4), e85987.

Gan, L., Li, W., Ma, Q., Artemyev, A. V. & Albert, J. M. 2022 Dependence of Nonlinear Effects on Whistler-Mode Wave Bandwidth and Amplitude: A Perspective From Diffusion Coefficients. *Journal of Geophysical Research (Space Physics)* **127** (5), e30063.

Hsieh, Y.-K., Kubota, Y. & Omura, Y. 2020 Nonlinear evolution of radiation belt electron fluxes interacting with oblique whistler mode chorus emissions. *Journal of Geophysical Research: Space Physics* p. e2019JA027465, e2019JA027465 2019JA027465, arXiv: https://agupubs.onlinelibrary.wiley.com/doi/pdf/10.1029/2019JA027465.

Hsieh, Y.-K. & Omura, Y. 2017*a* Nonlinear dynamics of electrons interacting with oblique whistler mode chorus in the magnetosphere. *J. Geophys. Res.* **122**, 675–694.

Hsieh, Y.-K. & Omura, Y. 2017*b* Study of wave-particle interactions for whistler mode waves at oblique angles by utilizing the gyroaveraging method. *Radio Science* **52** (10), 1268–1281, 2017RS006245.

Hull, A. J., Muschietti, L., Le Contel, O., Dorelli, J. C. & Lindqvist, P. A. 2020 MMS Observations of Intense Whistler Waves Within Earth's Supercritical Bow Shock: Source Mechanism and Impact on Shock Structure and Plasma Transport. *Journal of Geophysical Research (Space Physics)* **125** (7), e27290.

Hull, A. J., Muschietti, L., Oka, M., Larson, D. E., Mozer, F. S., Chaston, C. C., Bonnell, J. W. & Hospodarsky, G. B. 2012 Multiscale whistler waves within Earth's perpendicular bow shock. *J. Geophys. Res.* **117**, 12104.

Inan, U. S., Bell, T. F. & Helliwell, R. A. 1978 Nonlinear pitch angle scattering of energetic electrons by coherent VLF waves in the magnetosphere. *J. Geophys. Res.* **83** (A7), 3235–3254.

Itin, A. P., Neishtadt, A. I. & Vasiliev, A. A. 2000 Captures into resonance and scattering on resonance in dynamics of a charged relativistic particle in magnetic field and electrostatic wave. *Physica D: Nonlinear Phenomena* **141**, 281–296.

Karpman, V. I. 1974 Nonlinear Effects in the ELF Waves Propagating along the Magnetic Field in the Magnetosphere. *Space Sci. Rev.* **16**, 361–388.

Karpman, V. I., Istomin, J. N. & Shklyar, D. R. 1974 Nonlinear theory of a quasi-monochromatic whistler mode packet in inhomogeneous plasma. *Plasma Physics* **16**, 685–703.

Karpman, V. I. & Shklyar, D. R. 1977 Particle precipitation caused by a single whistler-mode wave injected into the magnetosphere. *Plan. Sp. Sci.* **25**, 395–403.

Katoh, Y. & Omura, Y. 2016 Electron hybrid code simulation of whistler-mode chorus generation with real parameters in the Earth's inner magnetosphere. *Earth, Planets, and Space* **68** (1), 192.

Kennel, C. F. & Engelmann, F. 1966 Velocity Space Diffusion from Weak Plasma Turbulence in a Magnetic Field. *Physics of Fluids* **9**, 2377–2388.

Landau, L. D. & Lifshitz, E. M. 1988 *Vol. 1: Mechanics*. Oxford: Pergamon.

Le Contel, O., Roux, A., Jacquey, C., Robert, P., Berthomier, M., Chust, T., Grison, B., Angelopoulos, V., Sibeck, D., Chaston, C. C., Cully, C. M., Ergun, B., Glassmeier, K.-H., Auster, U., McFadden, J., Carlson, C., Larson, D., Bonnell, J. W., Mende, S., Russell, C. T., Donovan, E., Mann, I. & Singer, H. 2009 Quasi-parallel whistler mode waves observed by THEMIS during near-earth dipolarizations. *Annales Geophysicae* **27**, 2259–2275.

Le Queau, D. & Roux, A. 1987 Quasi-monochromatic wave-particle interactions in magnetospheric plasmas. *Solar Physics* **111**, 59–80.

Li, W., Ma, Q., Shen, X. C., Zhang, X. J., Mauk, B. H., Clark, G., Allegrini, F., Kurth, W. S., Hospodarsky, G. B., Hue, V., Gladstone, G. R., Greathouse, T. K. & Bolton, S. J. 2021 Quantification of Diffuse Auroral Electron Precipitation Driven by Whistler Mode Waves at Jupiter. *Geophys. Res. Lett.* **48** (19), e95457.

Li, W., Thorne, R. M., Ma, Q., Ni, B., Bortnik, J., Baker, D. N., Spence, H. E., Reeves, G. D., Kanekal, S. G., Green, J. C., Kletzing, C. A., Kurth, W. S., Hospodarsky, G. B., Blake, J. B., Fennell, J. F. & Claudepierre, S. G. 2014 Radiation belt electron acceleration by chorus waves during the 17 March 2013 storm. *J. Geophys. Res.* **119**, 4681–4693.

Lyons, L. R. & Williams, D. J. 1984 *Quantitative aspects of magnetospheric physics.*.

Ma, Q., Li, W., Bortnik, J., Thorne, R. M., Chu, X., Ozeke, L. G., Reeves, G. D., Kletzing, C. A., Kurth, W. S., Hospodarsky, G. B., Engebretson, M. J., Spence, H. E., Baker, D. N., Blake, J. B., Fennell, J. F. & Claudepierre, S. G. 2018 Quantitative Evaluation of Radial Diffusion and Local Acceleration Processes During GEM Challenge Events. *Journal of Geophysical Research (Space Physics)* **123** (3), 1938–1952.

Melnikov, V. F. & Filatov, L. V. 2020 Conditions for Whistler Generation by Nonthermal Electrons in Flare Loops. *Geomagnetism and Aeronomy* **60** (8), 1126–1131.

Menietti, J. D., Averkamp, T. F., Kurth, W. S., Imai, M., Faden, J. B., Hospodarsky, G. B., Santolik, O., Clark, G., Allegrini, F., Elliott, S. S., Sulaiman, A. H. & Bolton, S. J. 2021 Analysis of Whistler-Mode and Z-Mode Emission in the Juno Primary Mission. *Journal of Geophysical Research (Space Physics)* **126** (11), e29885.

Meredith, N. P., Horne, R. B., Sicard-Piet, A., Boscher, D., Yearby, K. H., Li, W. & Thorne, R. M. 2012 Global model of lower band and upper band chorus from multiple satellite observations. *J. Geophys. Res.* **117**, 10225.

Meredith, N. P., Horne, R. B., Thorne, R. M. & Anderson, R. R. 2003 Favored regions for chorus-driven electron acceleration to relativistic energies in the Earth's outer radiation belt. *Geophys. Res. Lett.* **30** (16), 160000–1.

Mourenas, D., Zhang, X.-J., Artemyev, A. V., Angelopoulos, V., Thorne, R. M., Bortnik, J., Neishtadt, A. I. & Vasiliev, A. A. 2018 Electron Nonlinear Resonant Interaction With Short and Intense Parallel Chorus Wave Packets. *J. Geophys. Res.* **123**, 4979–4999.

Mourenas, D., Zhang, X. J., Nunn, D., Artemyev, A. V., Angelopoulos, V., Tsai, E. & Wilkins, C. 2022 Short Chorus Wave Packets: Generation Within Chorus Elements, Statistics, and Consequences on Energetic Electron Precipitation. *Journal of Geophysical Research (Space Physics)* **127** (5), e30310.

Mozer, F. S., Bonnell, J. W., Halekas, J. S., Rahmati, A., Schum, G. & Vasko, I. V. 2021 Whistlers in the Solar Vicinity That Are Spiky in Time and Frequency. *Astrophys. J.* **908** (1), 26.

Neishtadt, A. I. 1999 On Adiabatic Invariance in Two-Frequency Systems. *in Hamiltonian Systems with Three or More Degrees of Freedom, ed. Simo C., NATO ASI Series C. Dordrecht: Kluwer Acad. Publ.* **533**, 193–213.

Neishtadt, A. I. & Vasiliev, A. A. 2006 Destruction of adiabatic invariance at resonances in slow fast Hamiltonian systems. *Nuclear Instruments and Methods in Physics Research A* **561**, 158–165, arXiv: arXiv:nlin/0511050.

Nunn, D. 1971 Wave-particle interactions in electrostatic waves in an inhomogeneous medium. *Journal of Plasma Physics* **6**, 291.

Nunn, D. 1974 A self-consistent theory of triggered VLF emissions. *Plan. Sp. Sci.* **22**, 349–378.

Nunn, D. 1986 A nonlinear theory of sideband stability in ducted whistler mode waves. *Plan. Sp. Sci.* **34**, 429–451.

Nunn, D. & Omura, Y. 2012 A computational and theoretical analysis of falling frequency VLF emissions. *J. Geophys. Res.* **117**, 8228.

Nunn, D., Zhang, X. J., Mourenas, D. & Artemyev, A. V. 2021 Generation of Realistic Short Chorus Wave Packets. *Geophys. Res. Lett.* **48** (7), e92178.

Oka, M., Otsuka, F., Matsukiyo, S., Wilson, L. B., I., Argall, M. R., Amano, T., Phan, T. D., Hoshino, M., Le Contel, O., Gershman, D. J., Burch, J. L., Torbert, R. B., Dorelli, J. C., Giles, B. L., Ergun, R. E., Russell, C. T. & Lindqvist, P. A. 2019 Electron Scattering by Low-frequency Whistler Waves at Earth's Bow Shock. *Astrophys. J.* **886** (1), 53.

Oka, M., Wilson, III, L. B., Phan, T. D., Hull, A. J., Amano, T., Hoshino, M., Argall, M. R., Le Contel, O., Agapitov, O., Gershman, D. J., Khotyaintsev, Y. V., Burch, J. L., Torbert, R. B., Pollock, C., Dorelli, J. C., Giles, B. L., Moore, T. E., Saito, Y., Avanov, L. A., Paterson, W., Ergun, R. E., Strangeway, R. J., Russell, C. T. & Lindqvist, P. A. 2017 Electron Scattering by High-frequency Whistler Waves at Earth's Bow Shock. *Astrophys. J. Lett.* **842**, L11.

Omura, Y., Furuya, N. & Summers, D. 2007 Relativistic turning acceleration of resonant

electrons by coherent whistler mode waves in a dipole magnetic field. *J. Geophys. Res.* **112**, 6236.

Omura, Y., Matsumoto, H., Nunn, D. & Rycroft, M. J. 1991 A review of observational, theoretical and numerical studies of VLF triggered emissions. *Journal of Atmospheric and Terrestrial Physics* **53**, 351–368.

Omura, Y., Miyashita, Y., Yoshikawa, M., Summers, D., Hikishima, M., Ebihara, Y. & Kubota, Y. 2015 Formation process of relativistic electron flux through interaction with chorus emissions in the Earth's inner magnetosphere. *J. Geophys. Res.* **120**, 9545–9562.

Page, B., Vasko, I. Y., Artemyev, A. V. & Bale, S. D. 2021 Generation of High-frequency Whistler Waves in the Earth's Quasi-perpendicular Bow Shock. *Astrophys. J. Lett.* **919** (2), L17.

Schulz, M. & Lanzerotti, L. J. 1974 *Particle diffusion in the radiation belts*. Springer, New York.

Shapiro, V. D. & Sagdeev, R. Z. 1997 Nonlinear wave-particle interaction and conditions for the applicability of quasilinear theory. *Physics Reports* **283**, 49–71.

Shi, X., Liu, T. Z., Angelopoulos, V. & Zhang, X.-J. 2020 Whistler Mode Waves in the Compressional Boundary of Foreshock Transients. *Journal of Geophysical Research (Space Physics)* **125** (8), e27758.

Shklyar, D. R. 2021 A Theory of Interaction Between Relativistic Electrons and Magnetospherically Reflected Whistlers. *Journal of Geophysical Research (Space Physics)* **126** (2), e28799.

Shklyar, D. R. & Matsumoto, H. 2009 Oblique Whistler-Mode Waves in the Inhomogeneous Magnetospheric Plasma: Resonant Interactions with Energetic Charged Particles. *Surveys in Geophysics* **30**, 55–104.

Solovev, V. V. & Shkliar, D. R. 1986 Particle heating by a low-amplitude wave in an inhomogeneous magnetoplasma. *Sov. Phys. JETP* **63**, 272–277.

Stix, T. H. 1962 *The Theory of Plasma Waves*.

Summers, D. & Omura, Y. 2007 Ultra-relativistic acceleration of electrons in planetary magnetospheres. *Geophys. Res. Lett.* **34**, 24205.

Tao, X., Bortnik, J., Albert, J. M., Liu, K. & Thorne, R. M. 2011 Comparison of quasilinear diffusion coefficients for parallel propagating whistler mode waves with test particle simulations. *Geophys. Res. Lett.* **38**, 6105.

Tao, X., Bortnik, J., Albert, J. M. & Thorne, R. M. 2012*a* Comparison of bounce-averaged quasi-linear diffusion coefficients for parallel propagating whistler mode waves with test particle simulations. *J. Geophys. Res.* **117**, 10205.

Tao, X., Bortnik, J., Albert, J. M., Thorne, R. M. & Li, W. 2013 The importance of amplitude modulation in nonlinear interactions between electrons and large amplitude whistler waves. *Journal of Atmospheric and Solar-Terrestrial Physics* **99**, 67–72.

Tao, X., Bortnik, J., Thorne, R. M., Albert, J. M. & Li, W. 2012*b* Effects of amplitude modulation on nonlinear interactions between electrons and chorus waves. *Geophys. Res. Lett.* **39**, 6102.

Tao, X., Zonca, F., Chen, L. & Wu, Y. 2020 Theoretical and numerical studies of chorus waves: A review. *Science China Earth Sciences* **63** (1), 78–92.

Thorne, R. M., Bortnik, J., Li, W. & Ma, Q. 2021 *Wave–Particle Interactions in the Earth's Magnetosphere*, chap. 6, pp. 93–108. American Geophysical Union (AGU).

Thorne, R. M., Li, W., Ni, B., Ma, Q., Bortnik, J., Chen, L., Baker, D. N., Spence, H. E., Reeves, G. D., Henderson, M. G., Kletzing, C. A., Kurth, W. S., Hospodarsky, G. B., Blake, J. B., Fennell, J. F., Claudepierre, S. G. & Kanekal, S. G. 2013 Rapid local acceleration of relativistic radiation-belt electrons by magnetospheric chorus. *Nature* **504**, 411–414.

Tong, Y., Vasko, I. Y., Artemyev, A. V., Bale, S. D. & Mozer, F. S. 2019 Statistical Study of Whistler Waves in the Solar Wind at 1 au. *Astrophys. J.* **878** (1), 41, arXiv: 1905.08958.

Trakhtengerts, V. Y. & Rycroft, M. J. 2008 *Whistler and Alfvén Mode Cyclotron Masers in Space*. Cambridge University Press.

Vainchtein, D., Zhang, X. J., Artemyev, A. V., Mourenas, D., Angelopoulos, V. & Thorne, R. M. 2018 Evolution of Electron Distribution Driven by Nonlinear Resonances

With Intense Field-Aligned Chorus Waves. *Journal of Geophysical Research (Space Physics)* **123** (10), 8149–8169, arXiv: 1806.00066.

Vedenov, A. A., Velikhov, E. & Sagdeev, R. 1962 Quasilinear theory of plasma oscillations. *Nuclear Fusion Suppl.* **2**, 465–475.

Verscharen, D., Chandran, B. D. G., Boella, E., Halekas, J., Innocenti, M. E., Jagarlamudi, V. K., Micera, A., Pierrard, V., Štverák, Š., Vasko, I. Y., Velli, M. & Whittlesey, P. L. 2022 Electron-Driven Instabilities in the Solar Wind. *Frontiers in Astronomy and Space Sciences* **9**, 951628, arXiv: 2206.10403.

Wilson, L. B., Koval, A., Szabo, A., Breneman, A., Cattell, C. A., Goetz, K., Kellogg, P. J., Kersten, K., Kasper, J. C., Maruca, B. A. & Pulupa, M. 2013 Electromagnetic waves and electron anisotropies downstream of supercritical interplanetary shocks. *J. Geophys. Res.* **118**, 5–16, arXiv: 1207.6429.

Yao, S. T., Shi, Q. Q., Zong, Q. G., Degeling, A. W., Guo, R. L., Li, L., Li, J. X., Tian, A. M., Zhang, H., Yao, Z. H., Fu, H. S., Liu, C. M., Sun, W. J., Niu, Z., Li, W. Y., Liu, Z. Y., Le Contel, O., Zhang, S., Xiao, C., Shang, W. S., Torbert, R. B., Ergun, R. E., Lindqvist, P. A. & Pollock, C. J. 2021 Low-frequency Whistler Waves Modulate Electrons and Generate Higher-frequency Whistler Waves in the Solar Wind. *Astrophys. J.* **923** (2), 216.

Zhang, X., Angelopoulos, V., Artemyev, A. V. & Liu, J. 2018*a* Whistler and Electron Firehose Instability Control of Electron Distributions in and Around Dipolarizing Flux Bundles. *Geophys. Res. Lett.* **45**, 9380–9389.

Zhang, X. J., Agapitov, O., Artemyev, A. V., Mourenas, D., Angelopoulos, V., Kurth, W. S., Bonnell, J. W. & Hospodarsky, G. B. 2020*a* Phase Decoherence Within Intense Chorus Wave Packets Constrains the Efficiency of Nonlinear Resonant Electron Acceleration. *Geophys. Res. Lett.* **47** (20), e89807.

Zhang, X.-J., Artemyev, A., Angelopoulos, V., Tsai, E., Wilkins, C., Kasahara, S., Mourenas, D., Yokota, S., Keika, K., Hori, T., Miyoshi, Y., Shinohara, I. & Matsuoka, A. 2022 Superfast precipitation of energetic electrons in the radiation belts of the Earth. *Nature Communications* **13**, 1611.

Zhang, X. J., Demekhov, A. G., Katoh, Y., Nunn, D., Tao, X., Mourenas, D., Omura, Y., Artemyev, A. V. & Angelopoulos, V. 2021 Fine Structure of Chorus Wave Packets: Comparison Between Observations and Wave Generation Models. *Journal of Geophysical Research (Space Physics)* **126** (8), e29330.

Zhang, X. J., Mourenas, D., Artemyev, A. V., Angelopoulos, V., Bortnik, J., Thorne, R. M., Kurth, W. S., Kletzing, C. A. & Hospodarsky, G. B. 2019 Nonlinear Electron Interaction With Intense Chorus Waves: Statistics of Occurrence Rates. *Geophys. Res. Lett.* **46** (13), 7182–7190.

Zhang, X. J., Mourenas, D., Artemyev, A. V., Angelopoulos, V., Kurth, W. S., Kletzing, C. A. & Hospodarsky, G. B. 2020*b* Rapid Frequency Variations Within Intense Chorus Wave Packets. *Geophys. Res. Lett.* **47** (15), e88853.

Zhang, X. J., Thorne, R., Artemyev, A., Mourenas, D., Angelopoulos, V., Bortnik, J., Kletzing, C. A., Kurth, W. S. & Hospodarsky, G. B. 2018*b* Properties of Intense Field-Aligned Lower-Band Chorus Waves: Implications for Nonlinear Wave-Particle Interactions. *Journal of Geophysical Research (Space Physics)* **123** (7), 5379–5393.

Zhang, Y., Matsumoto, H., Kojima, H. & Omura, Y. 1999 Extremely intense whistler mode waves near the bow shock: Geotail observations. *J. Geophys. Res.* **104**, 449–462.